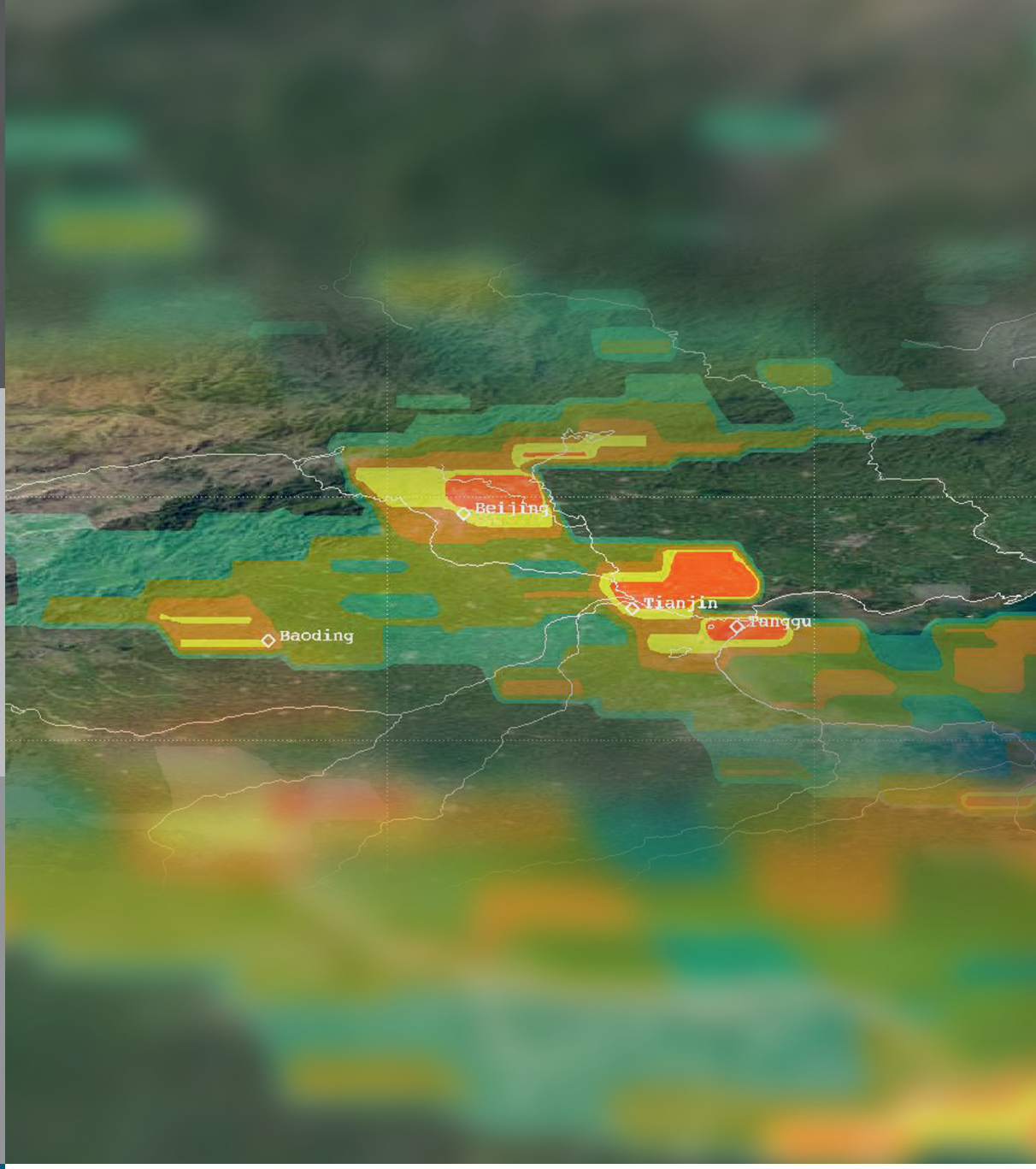

CITYZEN Climate Impact Studies

Martin Schultz (Editor)

Mitglied der Helmholtz-Gemeinschaft

JÜLICH
FORSCHUNGSZENTRUM

Schriften des Forschungszentrums Jülich
Reihe Energie & Umwelt / Energy & Environment Band / Volume 116

Forschungszentrum Jülich GmbH
Institut für Energie- und Klimaforschung (IEK)
Troposphäre (IEK-8)

CITYZEN Climate Impact Studies

Martin Schultz (Editor)

Schriften des Forschungszentrums Jülich
Reihe Energie & Umwelt / Energy & Environment Band / Volume 116

ISSN 1866-1793 ISBN 978-3-89336-729-0

Bibliographic information published by the Deutsche Nationalbibliothek.
The Deutsche Nationalbibliothek lists this publication in the Deutsche Nationalbibliografie; detailed bibliographic data are available in the Internet at http://dnb.d-nb.de.

Publisher and Distributor:	Forschungszentrum Jülich GmbH Zentralbibliothek 52425 Jülich Phone +49 (0) 24 61 61-53 68 · Fax +49 (0) 24 61 61-61 03 e-mail: zb-publikation@fz-juelich.de Internet: http://www.fz-juelich.de/zb
Cover Design:	Grafische Medien, Forschungszentrum Jülich GmbH
Source cover image:	Tropospheric Emission Monitoring Internet Service We acknowledge the free use of tropospheric NO2 column data from the OMI sensor from www.temis.nl.
Printer:	Grafische Medien, Forschungszentrum Jülich GmbH
Copyright:	Forschungszentrum Jülich 2011

Schriften des Forschungszentrums Jülich
Reihe Energie & Umwelt / Energy & Environment Band / Volume 116

ISSN 1866-1793
ISBN 978-3-89336-729-0

The complete volume ist freely available on the Internet on the Jülicher Open Access Server (JUWEL) at http://www.fz-juelich.de/zb/juwel

Table of Contents

1 Climate induced changes in air quality and chemical composition on different scales

Frode Stordal and Øivind Hodnebrog, University of Oslo, Norway

1.1 Abstract

We have estimated the impact of climate change on the chemical composition of the troposphere due to changes in climate from current climate (2000-2010) looking 40 years ahead (2040-2050). The climate projection has been made by the ECHAM5 model and was followed by chemistry-transport modelling using a global model, Oslo CTM2 (Isaksen et al., 2005; Søvde et al., 2008), and a regional model, EMEP. In this report we focus on carbon monoxide (CO) and surface ozone (O_3) which are measures of primary and secondary air pollution. In parallel we have estimated the change in the same air pollutants resulting from changes in emissions over the same time period.

1.2 Changes in climate from 2000-2010 to 2040-2050 predicted by ECHAM5

ECHAM5 has been run for this study in CityZen from year 2000 to year 2050. It was run using precalculated sea surface temperatures (SST) from a coupled climate model run with ECHAM5/MPIOM from the IPCC AR4 assuming emissions of greenhouse gases and aerosols according to scenario A1B (Nakicenovic et al., 2000). The A1 storyline and scenario family describes a future world of very rapid economic growth, global population that peaks in mid-century and declines thereafter, and the rapid introduction of new and more efficient technologies. Major underlying themes are convergence among regions, capacity building and increased cultural and social interactions, with a substantial reduction in regional differences in per capita income. The A1 scenario family develops into three groups that describe alternative directions of technological change in the energy system, where A1B assumes a balance across all energy sources. Temperatures increase in the 40 year period from 2000-2010 to 2040-2050 in the troposphere and decrease in the stratosphere, in agreement with known impacts of greenhouse gases (Figure 1). The warming, in Northern Hemisphere summer, was in general larger over continents than oceans, and with marked warming at high latitudes. There are also regions with cooling, most noticeably over the North Atlantic Ocean. In parts of Europe and China regional cooling from aerosols is evident, opposing the large scale warming due to the greenhouse gases. However, at mid latitudes there is in general a weaker warming than at both lower and higher latitudes, extending through most of the troposphere and even in both hemispheres.

As expected, a warmer troposphere in 2040-2050 has a higher specific moisture (Figure 2). This is most clearly seen in the tropics. The pattern of moistening to a large extent follows the pattern of warming, so that e.g. Europe will gain less moisture than northern Asia, and in China some regions will even be drier than during current conditions. Temperature changes impact chemistry directly as most chemical reactions are temperature dependent. Atmospheric moisture is important as OH is formed from water vapour.

Other parameters in the water cycle that impact the atmospheric chemistry are precipitation and cloud cover, regulating wet deposition of water soluble chemical species and thus radiative transfer and photo-dissociation rates respectively. Changes in these two parameters are clearly related to atmospheric moisture and also to each other, as seen in Fig-

ures 3 and 4. In the tropics the Hadley cell is somewhat displaced, yielding changes in tropical and subtropical precipitation and cloud cover. At low and mid latitudes, the fraction of mid and high level clouds decreases, whereas there is an increase in the fraction of low level clouds. The low level clouds increase their fraction in parts of Europe, whereas they decrease their fraction in other parts. Over India there is a noticeable decrease in precipitation as well as in cloud fraction. In China precipitation increases in the central and southern parts, whereas there is a drying in the north. Low level clouds follow the same pattern, with increased cloudiness in the south and decreased in the north.

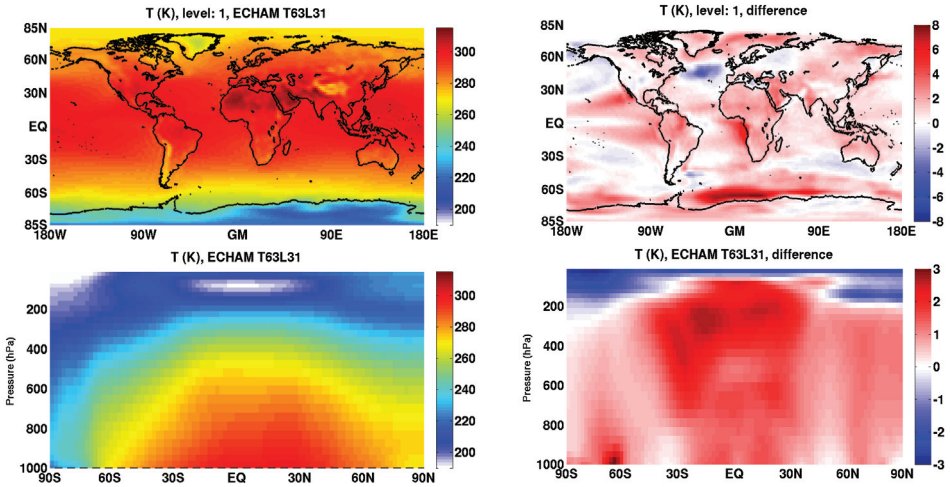

Figure 1: Temperature (K) as 11-year averages for the northern hemisphere summer (June, July, August) shown for the period 2000-2010 (left) and as differences between the periods 2040-2050 and 2000-2010 (right) for near-surface (top) and zonal mean (bottom). Note that the scales are different.

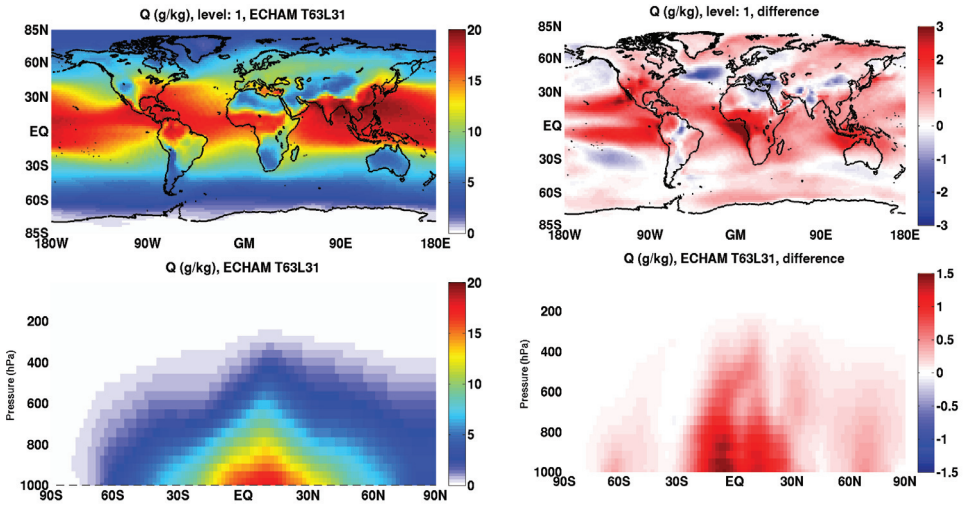

Figure 2: Specific humidity (g/kg) as 11-year averages for the northern hemisphere summer (June, July, August) shown for the period 2000-2010 (left) and as differences between the periods 2040-2050 and 2000-2010 (right) for near-surface (top) and zonal mean (bottom). Note that the scales are different.

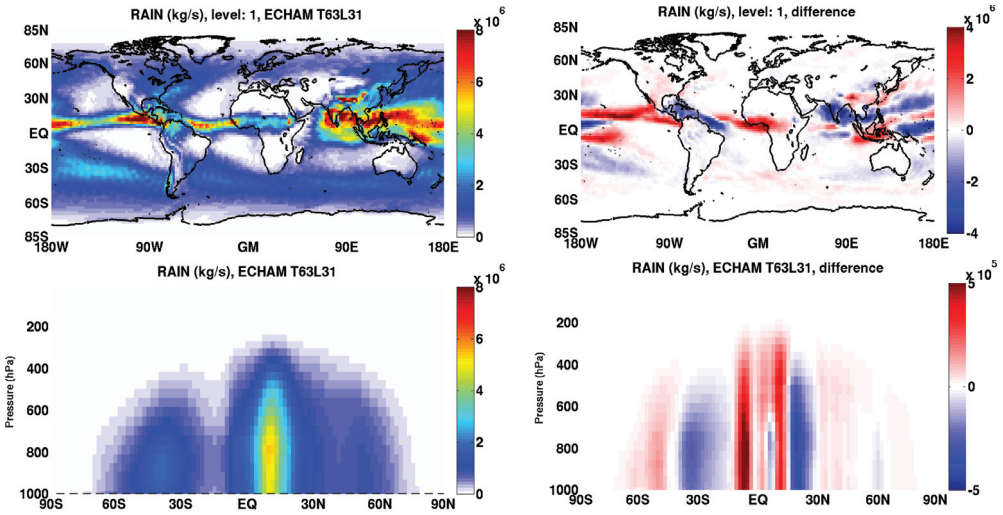

Figure 3: Precipitation flux (kg/s) as 11-year averages for the northern hemisphere summer (June, July, August) shown for the period 2000-2010 (left) and as differences between the periods 2040-2050 and 2000-2010 (right) for near-surface (top) and zonal mean (bottom). Note that the scales are different.

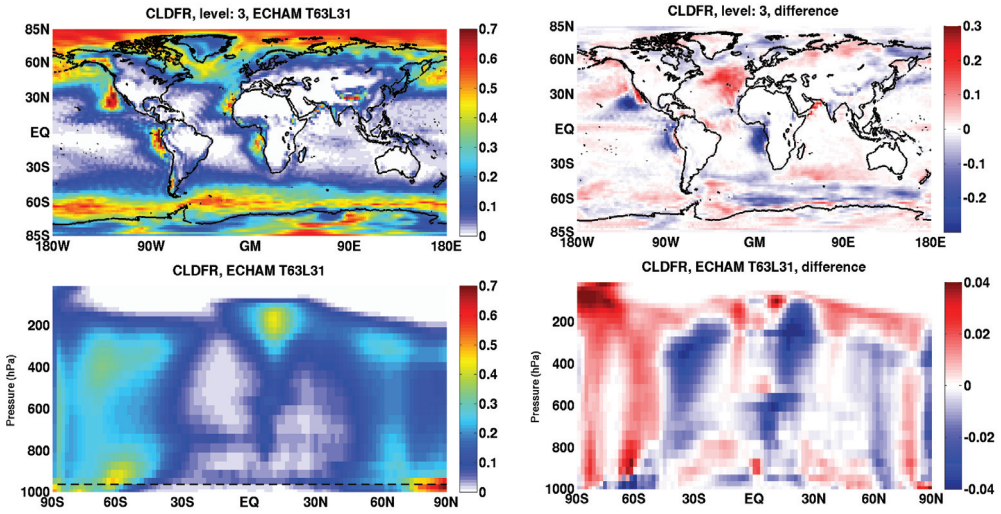

Figure 4: Cloud fraction (0-1) as 11-year averages for the northern hemisphere summer (June, July, August) shown for the period 2000-2010 (left) and as differences between the periods 2040-2050 and 2000-2010 (right) at the 950 hPa level (top) and in the zonal mean (bottom). Note that the scales are different.

1.3 Changes in anthropogenic emissions from 2005 to 2050

To put the changes in atmospheric chemistry due to climate change in perspective we have estimated also the changes in chemistry due to changes in anthropogenic emissions. We have selected the HIGH-CLE scenario developed by IIASA for this purpose. This scenario assumes full implementation of all current and planned air pollution legislation worldwide until 2030. Thus it provides a measure of the impact of current and planned air pollution policies. However, no specific climate or energy access policy is assumed.

We clearly see that in Europe emission legislation will result in continued reductions in emissions of CO as well as NOx in the 40 year period studied. All across Europe CO (Figure 5) and NOx (Figure 6) emissions are lower in 2040-2050 than in 2000-2010. We see the same negative trend in CO in China, but emissions of NOx are increasing slightly there. In many developing countries there will be increasing emissions of CO as well as NOx. This change is clearly evident for India (Figures 5 and 6).

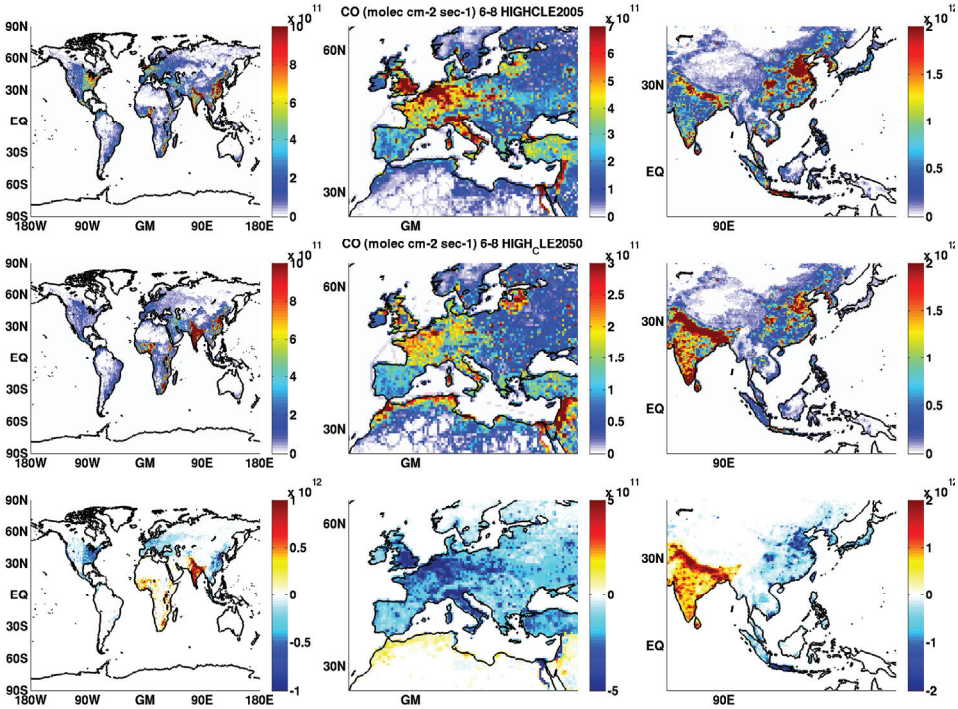

Figure 5: Anthropogenic emissions of CO (molec cm^{-2} s^{-1}) in the period June-August for 2005 (top), for 2050 HIGH CLE (middle), and as differences between the two scenarios (bottom). Note that the scales are different.

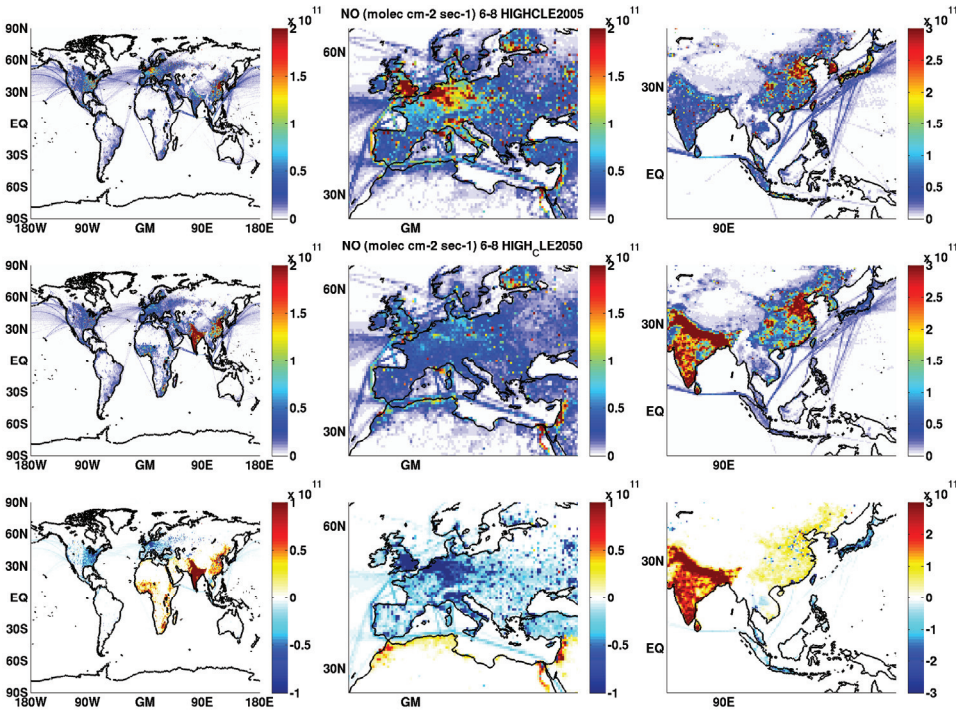

Figure 6: Anthropogenic emissions of NO_X (molec cm^{-2} s^{-1}) in the period June-August for 2005 (top), for 2050 HIGH CLE (middle), and as differences between the two scenarios (bottom). Note that the scales are different.

1.4 Changes in CO predicted by the OsloCTM2 model

The Oslo CTM2 model has been run with ECHAM as the meteorological driver. In the past this CTM has only been run with meteorology from the ECMWF. The capability to use ECHAM meteorology has been developed as a part of CityZen. We have run the model both for current (2000-2010) and future (2040-2050) meteorologies. The current conditions were run with both current and future emissions, whereas the future meteorology was run with future emissions, to allow separation of changes in the atmospheric chemistry which are due to the two changes. The estimated changes in CO concentrations are quite similar to the changes in the emissions themselves, at least at the surface which is depicted in Figure 7. However, at higher tropospheric levels the winds are stronger, so that the impacts of anthropogenic emission changes are advected some distance away from the emission changes themselves. The reductions in emissions over Europe lead to similar reduction in CO concentrations there. In a similar way concentrations of CO are reduced over China, but enhanced over India.

Interestingly, the response to climate change is an increase in CO concentration over the wetter parts of Europe and China: This is in contradiction to the fact that the atmospheric moisture content is higher, which would by itself lead to higher concentrations of OH. Likewise, the drying of northern China and northern India leads to decrease in CO concentrations there. Thus, the changes in CO surface concentrations are presumably influenced by also changes in the cloud fraction, with more cloudiness in the wetter regions and less in the drier ones, increasing the production of OH in the drier regions. Figure 7 shows that the signal in CO is stronger from emission changes than from climate changes. This can be seen also in the combined effect, which has a pattern more similar to changes in emissions than climate change. Nevertheless, the impact of climate change is noticeable, and must clearly be taken into account when assessing future CO concentrations in Europe and also other densely populated regions of the world.

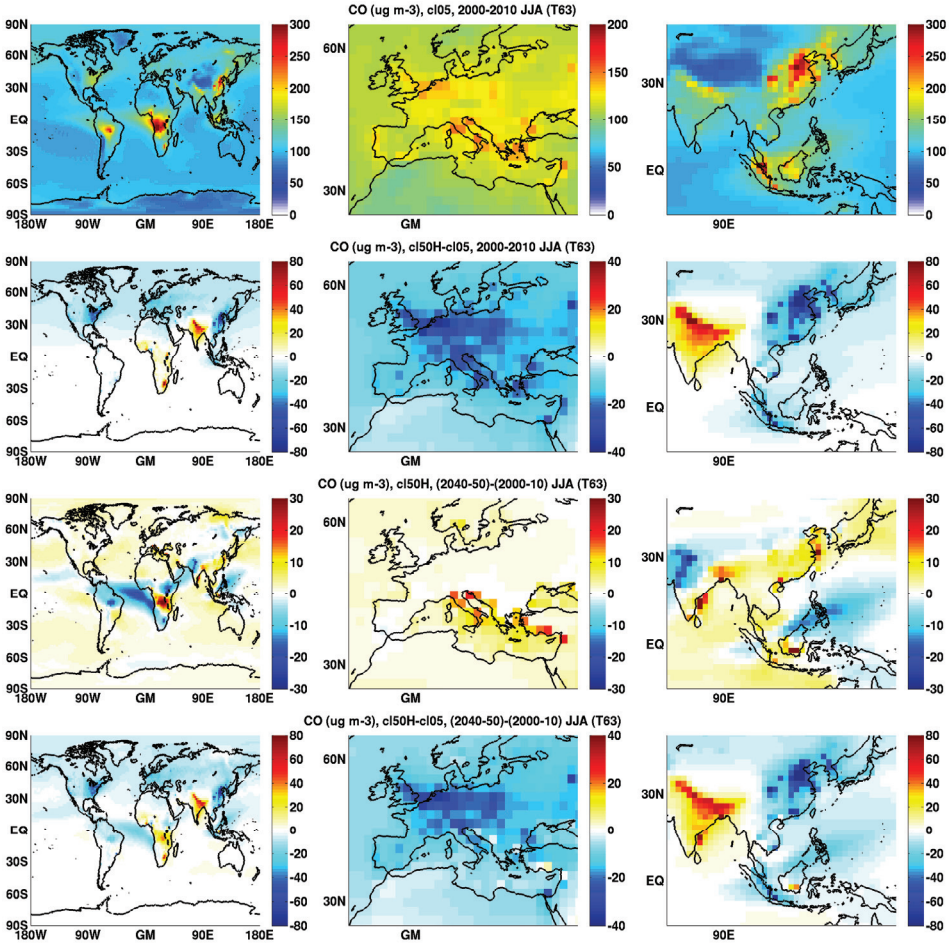

Figure 7: Near-surface CO (µg/m^3) for the northern hemisphere summer (June, July, August), for (i) 2000-2010 conditions (uppermost row); (ii) change due to changes in emissions from 2005 to 2050, the HIGH CLE scenario (second row); (iii) change due to change in climate in the period 2040-2050 (third row); (iv) and the change due to the combined impact of changes in emissions and climate (fourth row).

1.5 Changes in ozone predicted by the OsloCTM2 model

The ozone concentrations have been estimated in the same experiments as for CO and the results are shown in Figure 8. As the focus is here on air pollution we concentrate on the daily maximum value of the near surface concentrations. Like the concentrations of CO, ozone responds with reduced concentrations to changes in emissions in 2040-2050. In India, there is in a similar way increase in ozone as emissions increase for both CO and NOx. In China, we assume reductions in CO emissions but enhanced NOx emissions. The result is only weaker changes in ozone, with increase in some and decrease in other regions.

The climate response in ozone is increased surface maximum concentrations over much of the continental parts of the world. The impact of climate change is very complex, involving all the meteorological parameters discussed above, and even more, e.g. the boundary layer depth and mixing. In Europe, the largest increases in ozone are found in the Mediterranean region, with some hot spots which could be attributed to forest fires. The fires are assumed to have similar geographical and temporal distributions in the future (2040-2050) world, and apparently the meteorology is changed when we assume fires in the future. This particular feature is not realistic as the conditions for setting up fires will also change. However, what is not taken into account in our calculations is the fact that fire probability will increase in a future dries Mediterranean region. Thus our estimate are probably lower limit values. In Figure 9 we depict the year to year variability in surface ozone daily maximum. We see that the increase in ozone in the Mediterranean region is somewhat larger than the interannual variability. Ozone increases also in much of southern and central China as well as the southern and eastern parts of India. Like in the case of CO, the impacts of changes in emissions are somewhat more pronounced that those due to climate change. Consequently in the combined effect we recognize the emission effect most clearly. However, the impact of climate change is clearly noticeable, and must be taken into account when assessing future impacts on e.g. human health and agricultural production

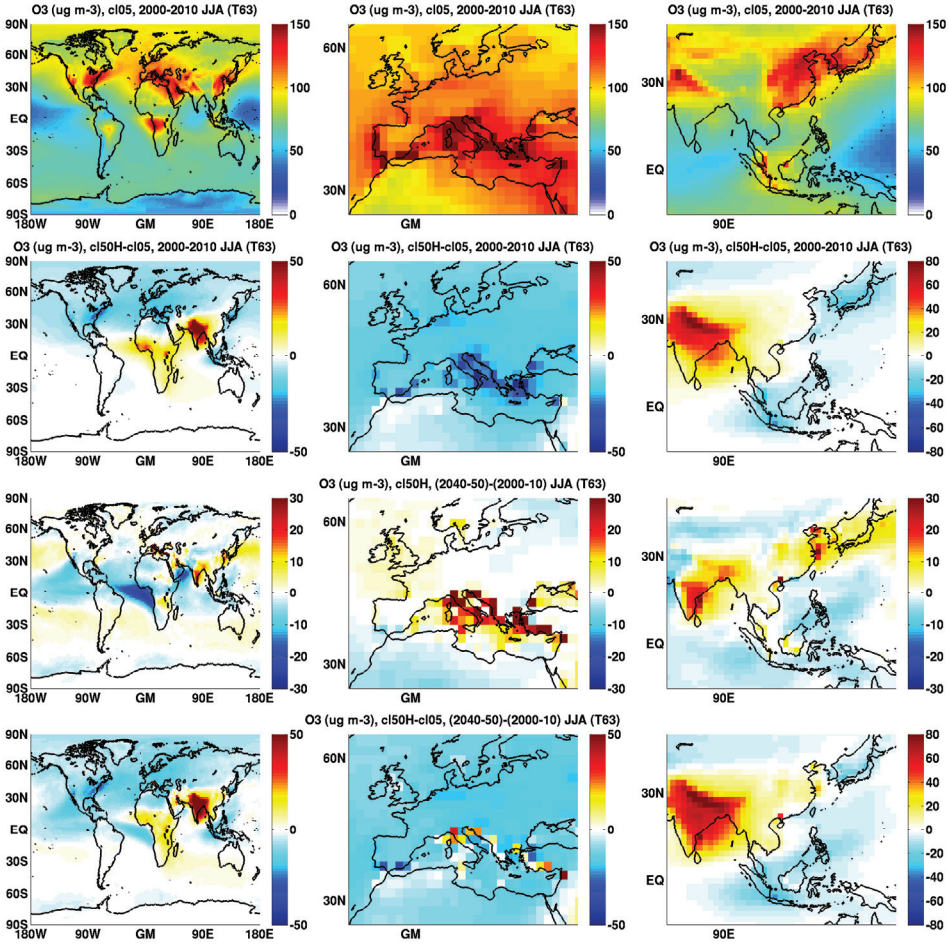

Figure 8: Near-surface ozone (µg/m^3) for the northern hemisphere summer (June, July, August), for (i) 2000-2010 conditions (uppermost row); (ii) change due to changes in emissions from 2005 to 2050, the HIGH CLE scenario (second row); (iii) change due to change in climate in the period 2040-2050 (third row); (iv) and the change due to the combined impact of changes in emissions and climate (fourth row). All estimates are for daily maximum ozone.

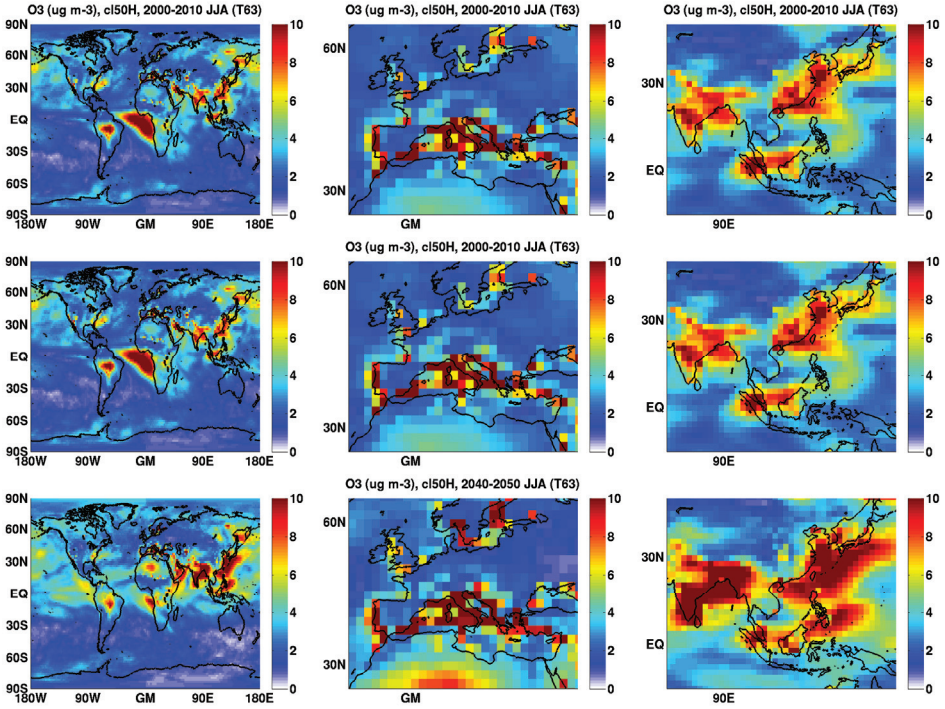

Figure 9: Absolute standard deviation over 11 years in near-surface ozone (µg/m^3) for the northern hemisphere summer (June, July, August), for (i) 2000-2010 conditions (uppermost row); (ii) 2000-2010 conditions with emissions from 2050, the HIGH CLE scenario (second row); and (iii) 2040-2050 conditions with emissions from 2050, the HIGH CLE scenario (third row). All estimates are for daily maximum ozone.

1.6 References

Isaksen, I. S. A., Zerefos, C., Kourtidis, K., Meleti, C., Dalsoren, S. B., Sundet, J. K., Grini, A., Zanis, P., and Balis, D.: Tropospheric ozone changes at unpolluted and semipolluted regions induced by stratospheric ozone changes, J. Geophys. Res.-Atmos., 110 (D2), 10.1029/2004jd004618, 2005.

Nakicenovic, N., Davidson, O., Davis, G., Grübler, A., Kram, T., La Rovere, E. L., Metz, B., Morita, T., Pepper, W., Pitcher, H., Sankovski, A., Shukla, P., Swart, R., Watson, R., and Dadi, Z.: Special Report on Emissions Scenarios, Cambridge University Press, Cambridge, 599 pp, 2000.

Søvde, O. A., Gauss, M., Smyshlyaev, S. P., and Isaksen, I. S. A.: Evaluation of the chemical transport model Oslo CTM2 with focus on arctic winter ozone depletion, J. Geophys. Res.-Atmos., 113 (D9), 10.1029/2007jd009240, 2008.

2 Impact of emission changes on climate

Cornelia Richter and Martin Schultz, IEK-8, Forschungszentrum Jülich, Germany

2.1 Introduction

There is no doubt any longer that anthropogenic emissions from fossil fuel burning, deforestation and other processes are leading to global warming (IPCC, 2007). Less certainty exists about the consequences of climate change, but there are a number of "fingerprints" which are likely associ-ated with climate change and begin to be observable even now:

1. Changes in precipitation patterns may lead to extended droughts in several regions of the world (e.g. Eastern Africa, central North America). There are real dangers that water supply in these areas will not sustain human settlement in the future. In other regions, precipitation is likely to increase, mainly in the form of massive precipitation events which cause flooding and damages to crops, buildings and infrastructure.
2. Warmer and drier summers, as predicted for central Europe for example, are likely to cause more frequent severe heat waves with elevated death toll as in the example of the summer 2003 event.
3. The warming of sea water and the melting of land ice causes the sea level to rise. Coastal areas and small islands will be prone to flooding and they will be more vulnerable to storm tides. This affects large numbers of people, because coastal areas have become densely populated during the 20th century.
4. The melting of glaciers will reduce freshwater supply in some areas thereby threatening or aggravating the sustainability of drinking water and agricultural water use. While water availability throughout the year may sometimes remain almost unchanged, alterations in the seasonal cycle might bear similar consequences when prolonged drought episodes become more frequent.

Currently, about 7% of the world's population lives in agglomerations with more than 10 million inhabitants (source: Thomas Brinkhoff: The Principal Agglomerations of the World, http://www.citypopulation.de, as of April 2011). Several of these megacities are located in regions which are particularly prone to feel the consequences of climate change and the population of meg-acities is extremely dependent on the supply of freshwater. The urban heat island effect exacerbates the consequences of summer heat waves (see also: CityZen Milestone report M-2-4-1 and refer-ences therein, or (Deely et al., 2010). Climate change might also have an impact on the develop-ment of megacities themselves. Megacity growth rates will depend on the number of people who arrive from rural areas, for example because they have to abandon their land as a consequence of droughts. Conversely, city dwellers are also responsible for a significant share of the global greenhouse gas emissions. It is difficult to estimate the exact share of megacity emissions due to several conflicting factors:

1. Standard-of-living is often higher in megacities implying that more energy is consumed per inhabitant and more CO_2 emissions are generated.

2. Megacities import goods (in particular food) from other regions so that emissions gener-ated during the production of these goods should be counted as megacity emissions as well and simple emission estimates from rural areas will overestimate the contributions of the rural population.
3. Technology is often more advanced in cities, which means that (fossil) fuel is used more efficiently and fewer emissions are generated for the same amount of "work" done. How-ever, current emission inventories generally assume a uniform distribution of emission factors throughout a country or district.
4. Transportation pathways are longer in rural areas so that delivery of goods from A to B may generate more emissions outside of city regions. On the other hand the globalization of the economy has led to vastly increased transportation pathways for many goods and (mega)city inhabitants might consume more and different goods than the rural population so that they are responsible for a larger share of the (global) emissions from transportation.

Assessing the climate impacts on megacities and the effects of megacities on climate is therefore a very complex task which will require a lot more research than what could be accomplished in the CityZen project. Governments have realized that intelligent urban planning and adaption to climate change impacts are urgently needed in order to minimize the vulnerability of megacities and their contribution to climate change (see for example the German Federal Ministry of Education and Research programme "Research for Sustainable Development of the Megacities of Tomorrow – Energy and Climate Efficient Structures in Urban Growth Centres", http://www.emerging-megacities.org).

In this report we present results from two sensitivity studies performed with the ECHAM5-MOZ and ECHAM5-HAM chemistry climate models in order to assess the impacts of climate change on air quality (with a focus on Europe) and the impact of megacity emissions on the global distribution of aerosols and the resulting radiative forcing. Contrary to the expectation at the writing of the CityZen proposal, it was not possible to perform these simulations with the new version of the model (ECHAM6-HAMMOZ) which would have included more interactions between gas-phase chemistry and aerosols and additional feedbacks from chemistry on radiation. The following sec-tions provide a brief overview on tropospheric chemistry and aerosol processes which may help in the interpretation of the model results. We then chose to highlight the problem of statistical significance which is crucial for the analysis of trends and the assessment of likelihood of a specific phenomenon. Unfortunately, chemistry climate models are still very expensive to run so that there are practically no studies available which explore the uncertainties in a statistically robust manner. Next we describe and interpret the results from our simulations and finally we offer some conclusions.

2.2 Trace gases and atmospheric chemistry

Tropospheric oxidants and other air pollutants have much shorter lifetimes than the prominent greenhouse gas CO_2. Therefore their concentrations vary regionally and the impacts of these sub-stances on weather patterns and vice versa will carry regional signatures and may often not be visible on the global scale. Nonlinearities in atmospheric chemistry complicate the assessment of potential changes, in particular if projected changes in regional emissions are large. A prominent example in this context is the photochemical ozone production. A simplified scheme of tropospheric ozone formation is shown in Figure 1 (Richter, 2008).

Elevated ozone concentrations in the troposphere, part of the so called summer smog, are build during the degradation of volatile organic compounds (VOCs). The presence of sunlight and nitrogen oxides $NO_x = NO + NO_2$ as a catalyst are another prerequisite. The VOCs are oxidized by hy-droxyl radicals OH and from organic peroxy radicals RO_2. These organic peroxy as well as later on the hydroperoxy radicals HO2 react with nitrogen oxide NO. The peroxy radicals release an oxygen atom to become organic oxyl RO and hydroxyl radicals OH, respectively. The oxygen atom in turn is picked up by NO with nitrogen dioxide NO_2 as the product. The organic oxy radical decomposes, isomerizes, or reacts with oxygen. This results in a carbonyl product (organic compound with a C=O group being part of it) and a hydroperoxy radical. The nitrogen dioxide, which is built as a side product of the VOC degradation, is decomposed by a photon hν. NO is rebuilt and the separated oxygen atom O combines with an oxygen molecule O_2 to form ozone O_3.

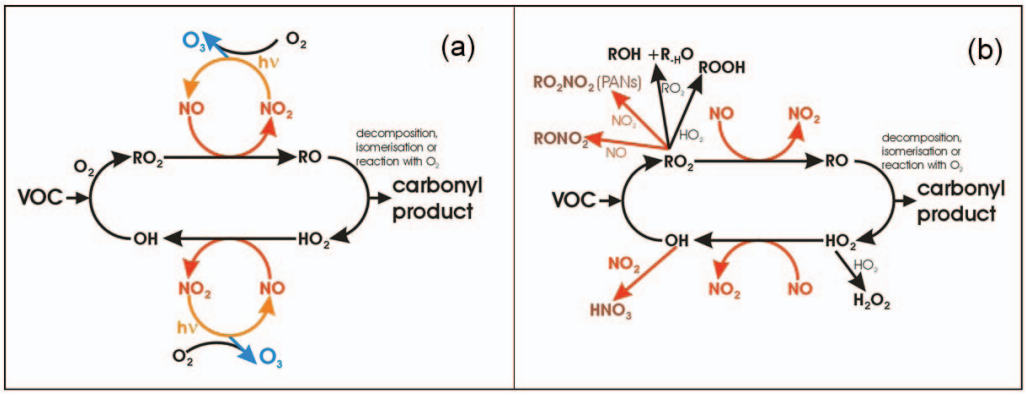

Figure 1: Photochemical ozone (O_3) production in the troposphere. (a) A chain reaction, which involves mainly anthropogenic nitrogen oxides ($NO_x = NO + NO_2$) and volatile organic compounds (VOCs), leads to the buildup of ozone O_3. Sunlight, symbolized as hν, is needed, to keep the cycle running. The VOCs are oxidized yielding carbonyl products. (b) Various chain termination reactions remove NO_x and/or the radicals (RO_2, HO_2, or OH) from the cycle. New radicals have to be build. Normally this happens by the photolysis of ozone, HONO, or aldehydes (not shown in the figure).

This chain reaction with the recycling of OH and NO is quite complex already. What makes things even more complicated are the chain termination reactions, which remove NO_x and radicals from the chain. For example adding NO_x to the system does not necessarily cause the cycle to run faster and accelerate the ozone build-up. The opposite, namely a deceleration of the ozone creation can happen, too, as among others the reaction of NO_2 with OH becomes more important then. Less OH is available for the initial step of the VOC degradation. The whole cycle runs slower. In contrast to naïve expectation, the increase of a precursor species lowers the ozone production rate in this so called VOC limited regime (low VOC to NO_x ratio). In this regime a lowering of the mainly anthropogenic NO_x emissions elevates the ozone production. In the NO_x limited regime (high VOC to NO_x ratio) however, a lowering of NO_x emissions reduces the ozone production. In the CityZen brochure available at https://wiki.met.no/cityzen/start the change of the regime of the London air pollution is illustrated. CityZen results on the influence of model resolution on this issue (low resolutions wipe out concentration peaks of trace gases due to the averaging over huge areas) are published in a recent CityZen publication (Hodnebrog et al., 2011).

2.3 Aerosols

Aerosols have natural and anthropogenic sources, can be emitted directly as particles (primary aerosols) or can form in the atmosphere from gaseous precursor species (secondary aerosols). Over sea and in costal areas, seasalt aerosols from sea spray are important. Mineral aerosols are particles picked up by wind from dry surfaces, especially surfaces without a shielding plant cover. Although these particles are rather big (diameters of 10µm and above), thus heavy compared to their surface and liable to gravity, they can reach quite far depending on the wind field. Sahara dust events in central Europe are one example for that. Marine and mineral aerosols belong to the coarse mode aerosols. In the CityZen focus of interest region Istanbul, the mass of seasalt and crustal particles made up nearly 20% of the observed mass in the period between November 2007 and June 2009 (Koçak et al., 2010). Volcanic eruptions are another important source of aerosols. Biogenic aerosols are particles produced by living organisms, e.g. pollens, fungi spores, bacteria, and viruses. Naturally occurring or humanly induced biomass burning is another temporally highly variable and massive source of (ash) aerosols. Human activities evoke emissions of primary aerosols, too. Fossil fuel combustion in various facilities like vehicles, power plants or for industrial purposes is the source for fine anthropogenic aerosols. Construction sites or abrasion at tires and brakes of road vehicles are sources for coarse aerosols. Gaseous precursor species, which may form secondary aerosols by nucleation or condense on pre existing particles, are emitted by the biosphere as well as by anthropogenic processes. An estimate of the global source strength as well as the global mean optical thickness at 550nm, which is a measure for the global load as well as the influence on the radiative budget of planet earth, is given in Table 1.

Table 1: Aerosol sources and global mean optical depths of aerosols according to the literature.

	Main sources for aerosol *Estimates of Andreae (1994)*	Approx. global emission flux [Tg / year]	Global mean optical thickness at 550 nm
Natural	***Primary aerosols***		
	Desert and semi-arid areas (mineral dust)	1500	0.023
	Marine sea spray	1300	0.003
	Volcanic dust	33	0.001
	Biogenic (pollens, debris)	50	0.002
	Secondary aerosols		
	Sulphates from biogenic gases	90	0.017
	Sulphates from volcanic SO_2	12	0.002
	Nitrates from nitrogen oxides	55	0.017
	Organics from volatile organic compounds (VOC)	22	0.001
	TOTAL	***~3060***	***0.066***
Anthropogenic	***Primary aerosols***		
	Industrial dust	100	0.004
	Soot	10	0.006
	Secondary aerosols		
	Organics from biogenic (VOC)	10	0.027
	Sulphates produced by SO_2	190	0.027
	Produced from biomass combustion gases	90	0.002
	Nitrates from nitrogen oxides	50	0.003
	TOTAL	***~390***	***0.069***

Aerosols from cloud condensation nuclei and as such influence the Earth's climate. One differ-entiates between direct aerosol effects on radiation (the scattering and absorption of solar and long-wave radiation on and by aerosol particles themselves) and indirect effects which are related to changes in cloud albedo (higher aerosol densities will lead to smaller cloud droplets which increase cloud brightness), cloud lifetime (smaller droplets are less likely to precipitate so that aerosol-rich clouds may live longer) and other feedbacks such as changes in buoyancy which affect the altitude to which clouds may rise.

2.4 A note on statistics

In order to assess climate change and its impacts it is not sufficient to only consider average quantities such as the global mean temperature. While these values can at times be meaningful, they often hide what is really happening and may imply consequences that are less harmful than they really are. One example from recent work under the task force of hemispheric transport of air pollu-tion (Fiore et al., 2009) are changes in surface ozone concentrations that are induced by moderate regional emission changes of ozone precursors. While annual average changes are generally very small, they hide the much larger compensating differences in summertime and wintertime ozone concentrations.

Figure 2 shows the probability density function of the Gauss distribution for three different mean values μ and standard deviations σ. Many atmospheric state variables exhibit frequency distributions that are very close to a gaussian distribution. The area under the curve between X0 and X1 rep-resents the probability of the random variable to assume a value between these limits (the total area is 1). An area of about 0.95 lies between -2σ to +2σ around the mean μ. This means that the random variable will fall into this range with a probability of 95% during a concrete experiment or observation. To phrase this differently: out of 100 simulated climate years, 5 years will show "atypical" results. Much smaller sample sizes (e.g. 10 years) are not sufficient to obtain a robust description of the statistical distribution and to assess if an observed change was indeed significant.

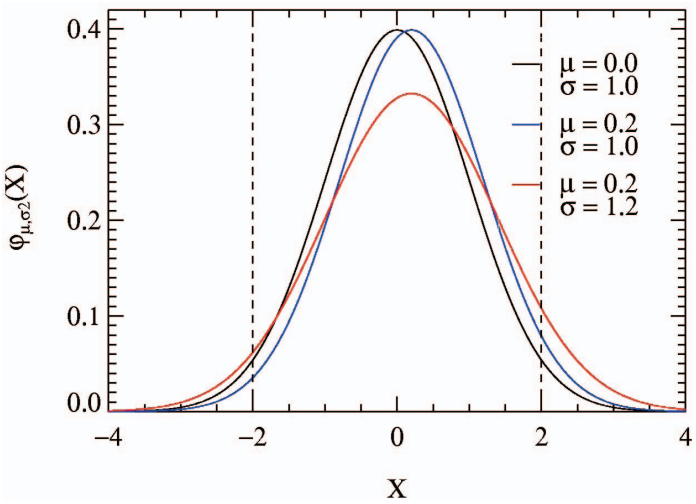

Figure 2 Probability density function φ of the Gauss distribution for three different pairs of mean values μ and standard deviation σ.

The accurate determination of the parameters of the distribution function is especially important to assess climate extremes. For example: The black curve in Figure 2 shows the standardized normal distribution with a mean value μ_0 of zero and a standard deviation σ_0 of one. The 2σ interval for this standardized normal distribution is marked with dashed lines. The probability for extreme events outside this interval is about 5% (2.5% for extreme values below $\mu_0-2\sigma_0$ and 2.5% for values above $\mu_0+2\sigma_0$). Increasing the mean value of the distribution shifts the distribution to higher values (blue curve). Extremely low values below $\mu_0-2\sigma_0$ are less probable for this case (the blue curve lies below the black), the probability for extremely high values above $\mu_0+2\sigma_0$ rises (blue curve is above the black). If not only the mean value rises but also the variability σ^2 (red curve), the probability for extreme events may rise not only at one end of the distribution but on both (red curve is above the black outside the $2\sigma_0$ interval). Referring to the example of temperature deviations this means that rising climate variability elevates the probability of extremely cold temperatures although the global mean temperature rises.

A high variability of observed climate or air quality variables makes it difficult to assess small trends in the time series of these variables. Long time series are needed to find "real" trends, which are statistically significant and not only a misinterpretation of interannual variability. This is demonstrated in **Figure 3**.

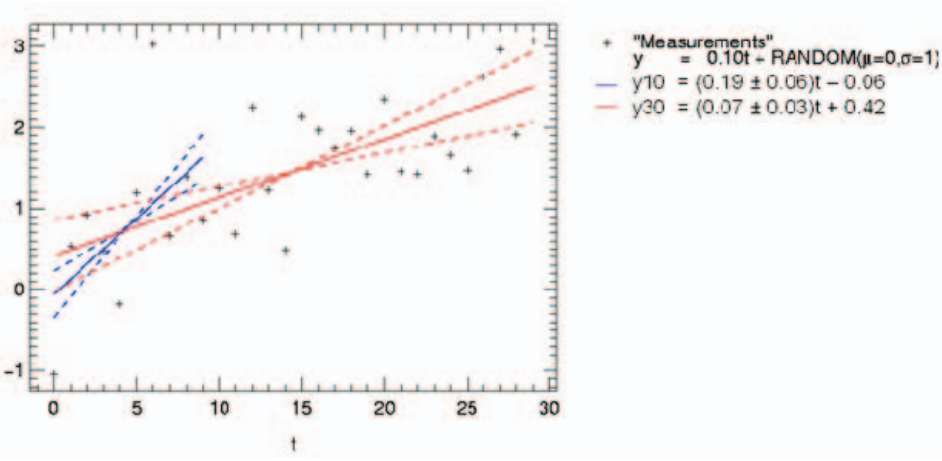

Figure 3 Regression lines in a highly variable fictitious timeseries. The timeseries has an underlying small trend (0.1 per timestep). If only a short interval (10 timesteps) is looked at, a quite different "trend" will be found compared to the one determined with the longer timeseries (30 timesteps).

The fictitious time series in Figure 3 was built by adding randomly normal distributed deviations ($\mu=0$, $\sigma=1$) to a small trend of 0.1 per time step. Two regression lines are deduced by a linear least square fit. The first one (blue) uses the first 10 time steps only. A much larger trend is found in this case. Actually the 95% confidence interval[1] of the fitting

[1] From the slope of the regression line b, the residual variance around this line s_b (assumed as being Gauss distributed), and a hypothesis for the slope b_0, the variable t_b can be defined, which is Student-T distributed. The Student-T distribution is a special probability density function, depending on degrees of freedom m. This degree of freedom depends on the sample size (number of measurements). For huge m it is equal to the Gauss distribution. By prescribing a significance level α (for a 95% confidence interval α=5%), a maximum and minimum for t can be calculated from the Student T distribution for m = n-2, with the number of used data points for the regression analysis being denoted as n. From this t_{max} and t_{min} values for b_{0max} and b_{0min} are derived giving the confidence interval for a prescribed α.

line's slope does not cover the underlying prescribed (real) gradient of the fictitious "measurements" in this example case. If 30 time steps are taken into account for the regression analysis, the slope of the fitting line is much closer to the real trend. The 95% confidence interval of the fitting line slope just covers this real trend. In reality, the underlying real trend is unknown, but has to be derived from the time series. The higher the residual variance around the fitting line, the longer time series are needed. If the reason for the residual variance is known and the effect of underlying process can be foreseen, thus it is not a random deviation from the trend line, this part of the variation should be removed. For example, if a time series shows a strong seasonality, it is appropriate to look at the trend of each season separately or to de-seasonalize the time series prior to the trend analysis. Additional complications arise if – as in the case of tropospheric ozone – there are indications that the trend is in fact non-linear.

2.5 Impacts of climate variability on air quality in Europe

In order to investigate the impact of weather patterns on air quality in Europe we carried out two long-term simulations covering the period 1989 to 2008 with the ECHAM5-MOZ chemistry climate model. One of the simulations (henceforth called "nudged run") was driven by assimilated meteorological fields (surface pressure, air temperature, vorticity and divergence) from the ERA-Interim reanalysis (ECMWF) while the other simulation was constrained only by a climatology of sea ice and sea surface temperatures ("unnudged run"). In the nudged simulation, the meteorological input fields are read every six hours and the climate state is relaxed towards these fields with e-folding times of 6 to 24 hours. The ECHAM5-MOZ model includes a comprehensive tropospheric trace gas chemistry package but does not account for prognostic aerosols. Meteorology affects trace gas concentrations through feedbacks on chemical reaction rates, photolysis frequencies, emissions, deposition and washout. There is no feedback from the tracer fields to the shortwave or longwave radiative transfer in the climate model.

2.5.1 ECHAM5-MOZ model description and simulation setup

The 3D global chemistry climate model ECHAM5-MOZ is part of the Max Planck Institute for Meteorology (Hamburg, Germany) earth system model. It consists of the atmospheric general circulation model ECHAM5 and the chemistry transport model MOZART2.

ECHAM5 is the 5th generation general circulation model of the Max Planck institute for Meteorology. It evolved from the ECMWF operational forecast model cycle 36 and a comprehensive physics parameterisation package. Details can be found in (Roeckner et al. 2003). The sensitivity of the ECHAM5 model to different horizontal (T21 - T159 sprectral triangular truncation) and vertical (L19 - L159 levels) resolutions concerning the simulated climate is dealt with in (Roeckner et al. 2006) and concerning tracer transport in (Aghedo et al. 2010). Besides chemistry tracers undergo advection, convective transport, and vertical diffusion as well as wet and dry deposition. For the advection a mass conserving semi Lagrangian transport scheme (Lin and Rood, 1996) on a Gaussian grid is used. Convective transport is parameterized as proposed by (Tiedtke, 1989) with modifications following (Nordeng, 1994). The parameterizations for the wet deposition are adapted from Seinfeld (Seinfeld and Pandis, 1998) and (Stier et al., 2005). The vertical diffusion is extended in ECHAM5-MOZ compared to ECHAM5 to include the net tracer flux of surface emissions minus dry deposition. The dry deposition of ozone, nitrogen oxides and nitric

acid vapour is implemented according to the resistance model of (Ganzeveld and Lelieveld, 1995).

The atmospheric chemistry scheme of MOZART2 (**M**odel of **OZ**one **A**nd **R**elated chemical **T**racers, version 2) used in ECHAM5-MOZ consists of 63 species representing ozone, nitrogen oxides and hydrocarbon chemistry in 168 reactions. The solver uses the Euler backward integration method. Details on the scheme can be found in (Horowitz et al. 2003). The photolysis rates are computed by interpolation from a multivariate table. This table originates from calculations with the **T**ropospheric **U**ltraviolet and **V**isible radiation model (TUV, version 3.0) (Madronich and Flocke 1999). The model does not simulate stratospheric chemistry explicitly but relaxes the concentrations of ozone to climatologies from (Logan 1999) for O_3 below 100 mb and the **HAL**ogen **O**ccultation **E**xperiment (HALOE) (Randel et al. 1998) for O_3 above 100 mb. The stratospheric concentrations of NO_x = NO + NO_2, HNO_3, N_2O_5, and N_2O are relaxed toward zonally and monthly averaged values from the middle atmosphere model **S**tudy of **T**ransport **A**nd Chemical **R**eactions in the **S**tratosphere (STARS) (Brasseur et al. 1997).

In this study ECHAM5-MOZ was run on a horizontal resolution of T63 (spectral triangular truncation), corresponding to a grid resolution of roughly 150km × 150km. The model has 31 vertical levels (L31) from the surface up to 10hPa. The nudged simulation was driven with analyzed fields of surface pressure, temperature, vorticity, divergence, sea surface temperature, and sea ice cover from ECMWF operational meteorological data in order to reproduce the weather patterns during the period 03 1989 -12 2008. In the unnudged simulation sea surface temperatures and sea ice coverage data were used from (Hurrell et al. 2008).

Anthropogenic trace gas emissions are taken from the ACCMIP inventory (Lamarque et al., 2010). Till the year 2000 the historic reanalysis data are used (the linear interpolation between the given decadal values), from the year 2001 on, the RCP8.5 scenario data are used (Riahi et al., 2007). Biogenic emissions from terrestrial vegetation are computed interactively with the Model of Emissions of Gases and Aerosols from Nature (MEGAN), version 1 (Guenther et al., 2006) using updated isoprene and terpene maps of potential emissions which resemble those of the MEGAN version 2 inventory. The NOx emissions by lightning are computed interactively based on convective updraught velocities following (Grewe et al., 2001). Methane concentrations in the model are constrained with a zonal mean surface climatology in the planetary boundary layer, so that time varying CH4 emissions (e.g. derived from inverse modelling using satellite retrievals (Bergamaschi et al., 2009) only serve to create spatial patterns near the surface.

2.5.2 Mean values of surface temperature and ozone

In **Figure 4** the simulated mean summer (June, July, August) temperatures are shown for the nudged and unnudged run, respectively. With the chosen color scale, the two fields look very similar, indicating that the model is able to capture the mean temperature distribution over Europe rather well in spite of its coarse resolution and the constraint by sea ice and sea surface temperature only. The largest exception occurs in the White Sea where the nudged simulation exhibits 3.5 degree warmer temperatures on average due to less sea ice coverage. The unnudged run is slightly cooler over the western part of the Baltic Sea, parts of France, the Alps and Russia. It is warmer over the Mediterranean and large parts of North Africa (Figure 5).

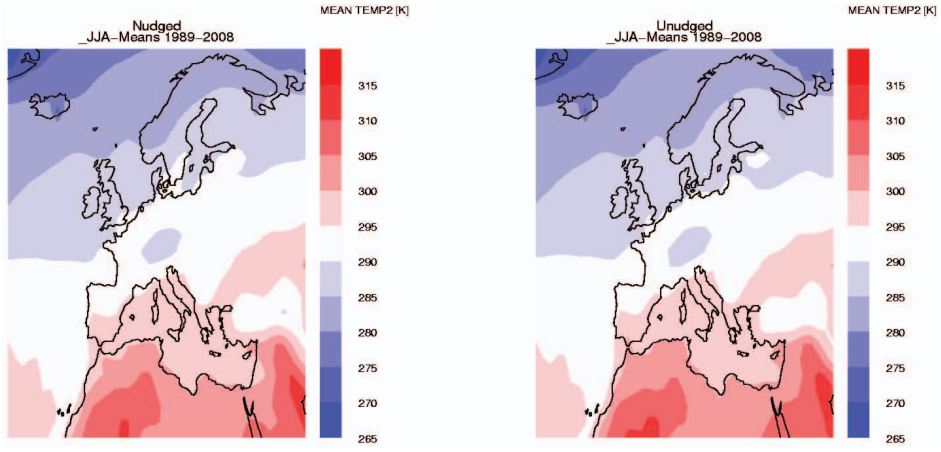

Figure 4 Mean summer 2m-temperature in the nudged (left) and unnudged (right) ECHAM5-HAM simulations.

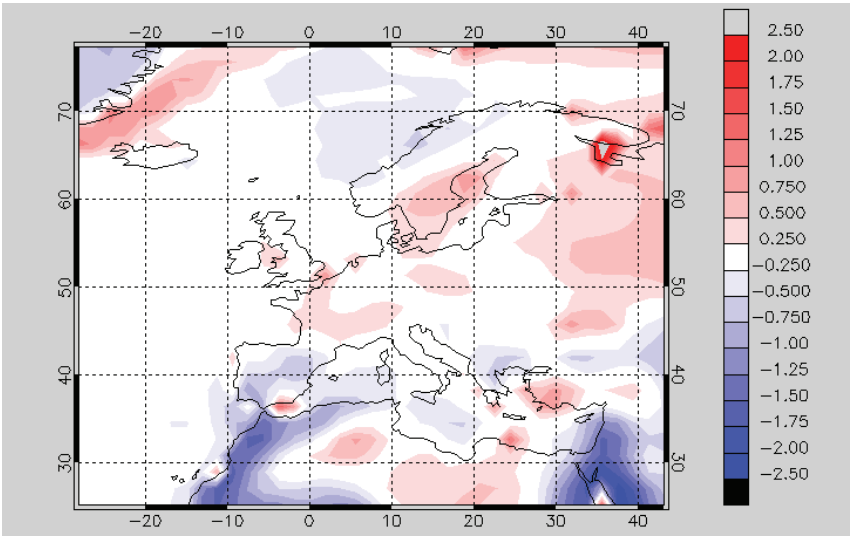

Figure 5 Difference of mean summer 2m-temperatures between the nudged and unnudged simulations [units: K].

Comparing the mean summer ozone concentrations shown in **Figure 6** again shows very good agreement between the two simulations. The unnudged simulation tends to yield slightly lower ozone concentrations. Both models agree in placing the highest ozone values in the Mediterranean Sea, where high anthropogenic and biogenic emissions coincide with high sunlight intensity. In contrast to the Eastern Mediterranean results obtained by other groups in the CityZen project, ECHAM5-MOZ does not show significantly larger ozone concentrations in the Eastern Mediterranean region compared to the western region.

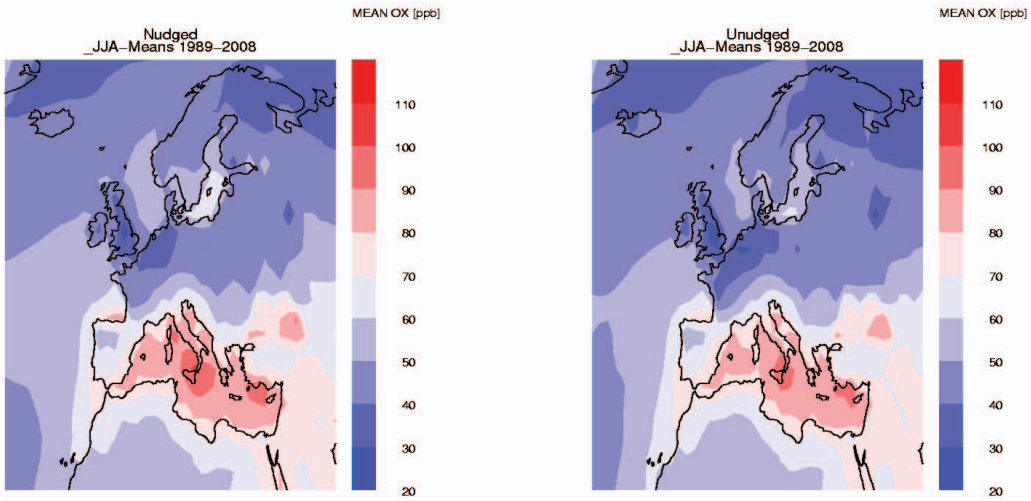

Figure 6 Mean summer surface Ox values. In the unnudged simulation (right) the values tend to be slightly lower.

Figure 7 shows the JJA 20-year mean difference of surface ozone concentrations between the two runs. The nudged simulation yields somewhat larger concentrations in particular in (but not limited to) regions where the average temperature is warmer (see Figure 5).

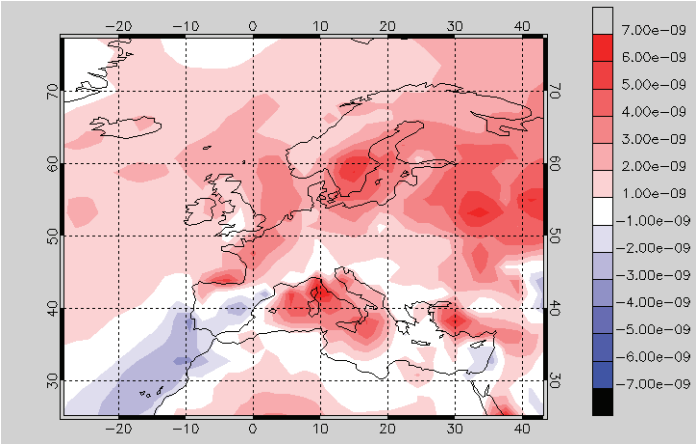

Figure 7 Difference between summer surface Ox values from the nudged and unnudged simulation [units: nmol mol-1].

2.5.3 Variability

Figure 8 shows the standard deviation of the mean summer temperatures in the nudged and unnudged simulation, respectively. Obviously, the geographical patterns are not equal. Again, the White Sea shows up as an outlier due to differing sea ice coverage. The unnudged simulation exhibits about twice the variability in Spain, southern France and northern Italy than the nudged run and the region of lower variability which stretches across France, Switzerland, Austria, Hungary etc. is shifted to the north.

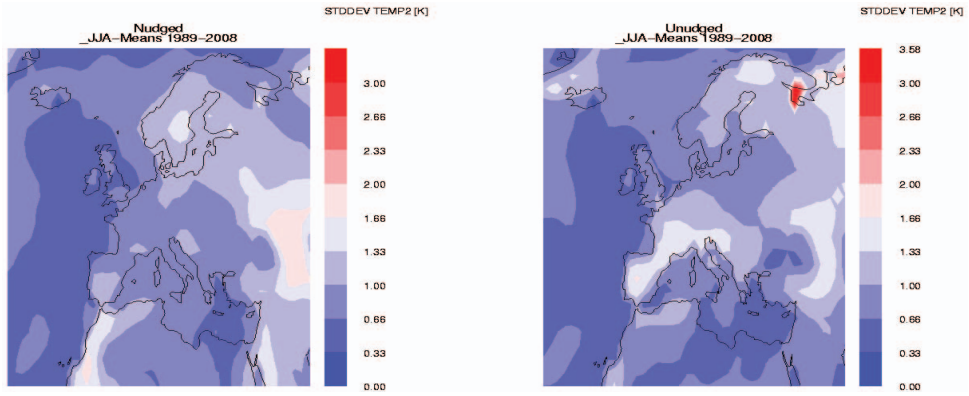

Figure 8 Standard deviation of the 2m-temperature in the summer month (JJA). Left: nudged simulation, right: unnudged run.

Figure 9 displays the difference between the mean 95%-ile and mean median 2m temperatures of the 1990s from the two runs. The 95%-ile and median values were computed from the 3-hourly output for each summer season (JJA) between 1990 and 1999 and then averaged. While the patterns of the "heat episodes" are comparable in the two simulations, the unnudged simulation exhibits somewhat stronger temperature enhancements than the nudged simulation. In theory this should also lead to higher maximum ozone concentrations. However, this is not confirmed (see Figure 7a below).

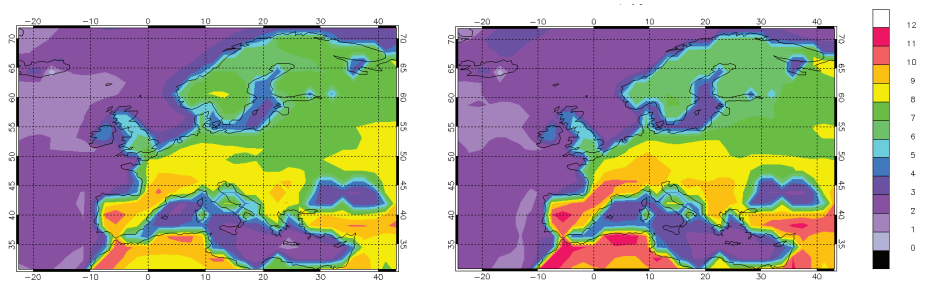

Figure 9 Summertime 2m-temperature enhancements expressed as difference between the mean 95%-ile and mean median values from the nudged (left) and unnudged (right) simulations. [units: K].

Fehler! Verweisquelle konnte nicht gefunden werden. shows the mean summer ozone concentration variability. In Eastern Europe, the variability is again underestimated. On the other hand, Figure 11 shows that both simulations yield rather similar "high ozone values", expressed here as 95%-iles computed from the 3-hourly model output. Both the regions and the absolute enhancements of ozone concentrations are very similar in the two runs. The same is true for the low end of the distribution (5%-ile plots in Figure 11).

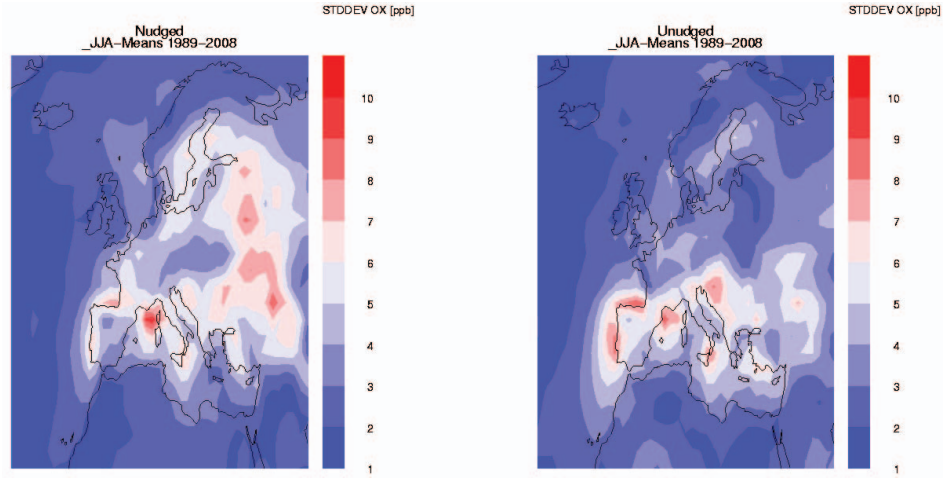

Figure 10 Mean summer ozone concentration variability. In Eastern Europe the variability is highly underestimated.

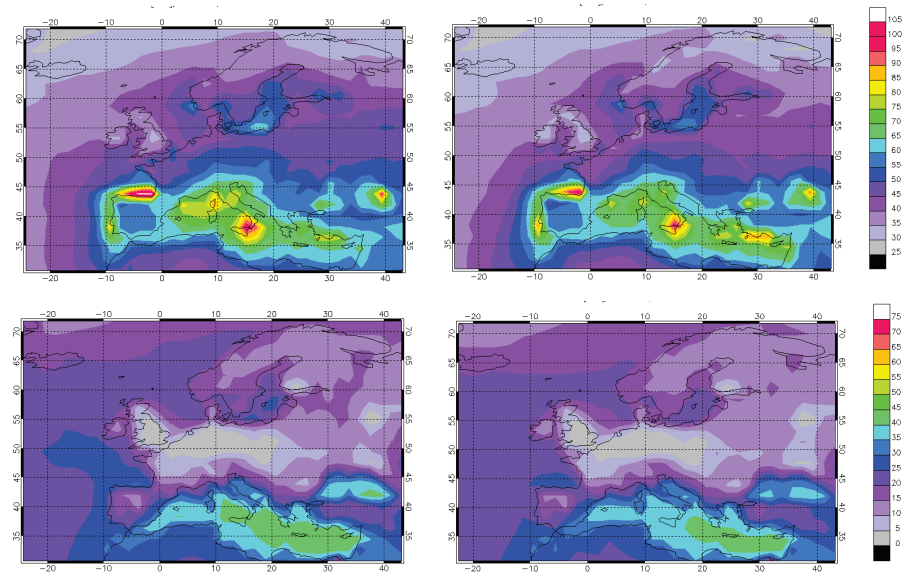

Figure 10 Average summertime 95%-iles (top) and 5%-iles (bottom) of the simulated surface ozone concentration during the 1990s in the nudged (left) and unnudged (right) simulations [units: ppbv].

2.5.4 Trends

Figure 12 shows the 2m-temperature trends for the summertime (JJA) mean values. Over large parts of central Europe, no significant trend can be detected in either of the simulations. A noticeable difference is the warming of the Iberian Peninsula that is predicted in the unnudged simulation but absent in the nudged simulation. The nudged run exhibits a much larger warming to the east of Europe, while the unnudged simulation shows greater temperature increases in the northern North Atlantic. There are practically no regions where temperature decreased over the past 20 years.

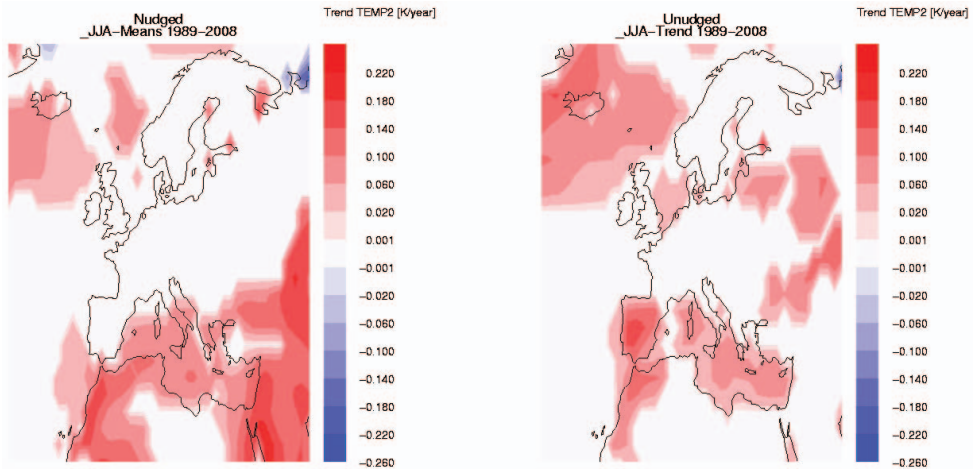

Figure 12 Statistically significant near surface mean summer temperature trends.

Looking at the ozone trends shows a different picture. In the nudged simulation a clear, significant negative trend is visible, whereas hardly any significant trend shows up in the unnudged simulation (Figure 13).

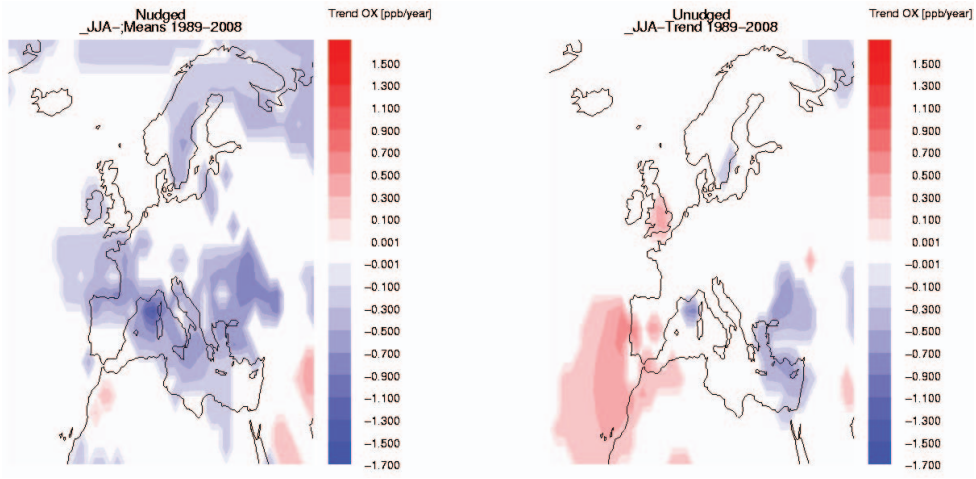

Figure 13 Significant summer ozone concentration trends.

2.6 ECHAM5-HAM sensitivity runs: How do aerosol emissions from megacities affect climate

Two ten year future (years 2025 – 2035, year 2025 as spin up) scenario simulations were done with the ECHAM5-HAM model. This model deals with aerosols in the atmosphere and their impact on weather elements and climate. A two way coupling is established in this model, thus the weather conditions do not only influence the aerosols' fate, but the aerosols change the weather conditions as well (see chapter **Fehler! Verweisquelle konnte nicht gefunden werden.**). By switching off the megacities' anthropogenic aerosol emissions in one of the ten year simulations, the influence of megacities on global climate (radiative forcing measures are calculated by the model, too) and on weather elements, especially cloud properties, could be looked at.

2.6.1 ECHAM5-HAM model description and simulation setup

The ECHAM5-HAM model consists of the same general circulation model ECHAM5 as the above described ECHAM5-MOZ. Instead of the chemistry transport model MOZART, the ECHAM5 is coupled with the Hamburg Aerosol Model HAM. The model is described in (Stier et al., 2005) in detail. Here only a short introduction is given.

For computational efficiency, the aerosol spectrum (see chapter **Fehler! Verweisquelle konnte nicht gefunden werden.**) is divided into seven modes (four soluble and three insoluble modes). They are classified as given in **Fehler! Verweisquelle konnte nicht gefunden werden.**2. Five different aerosol cpecies are considered, namely sulphate, black carbon, organic matter, dust and seasalt. The smallest fraction of particles in the model only consists of soluble sulfur (SU) particles. This fraction is called nucleation mode with particle radii below 0.005µm. In the Aitken mode with radii between 0.005 and 0.05 µm, sulfur, black carbon (BC) and particulate organic matter (POM) are dealt in the soluble / mixed state and additionally insoluble fractions of BC and POM. In the accumulation mode (0.05 – 0.5 µm), sulfur, black carbon, particulate organic matter, sea salt (SS) and dust (DU) particles are dealt in the soluble/mixed state and dust particles in the insoluble mode. In the coarse mode, radii above 0.5µm, the same particles as in the coarse mode are simulated.

Table 2 Aerosol modes in HAM. N_i denotes the aerosol number of mode i, M_{ij} the mass of mode i of compound j. The different compounds are: SU (sulfur), BC (black carbon), POM (particulate organic matter), SS (sea salt), and DU (dust). The mode borders are defined via the radius of the particles r. For some compounds not only soluble of mixed but also insoluble aerosols exist. The table is copied from (Stier et al. 2005).

Modes $\bar{r}$ [µm]	**Soluble / Mixed**	**Insoluble**
Nucleation		
$\bar{r} \leq 0.005$	N_1, M_1^{SU}	
Aitken		
$0.005 < \bar{r} \leq 0.05$	$N_2, M_2^{SU}, M_2^{BC}, M_2^{POM}$	N_5, M_5^{BC}, M_5^{POM}
Accumulation		
$0.05 < \bar{r} \leq 0.5$	$N_3, M_3^{SU}, M_3^{BC}, M_3^{POM}, M_3^{SS}, M_3^{DU}$	N_6, M_6^{DU}
Coarse		
$0.5 < \bar{r}$	$N_4, M_4^{SU}, M_4^{BC}, M_4^{POM}, M_4^{SS}, M_4^{DU}$	N_7, M_7^{DU}

Beside the direct emissions, particles undergo sedimentation, wet and dry deposition. In the microphysics module, nucleation (building of new particles from gaseous precursors), coagulation (combination of two or more preexisting particles), and condensation of gaseous tracers onto existing aerosols is treated.

The model was run in T63L31 resolution. As mentioned above, the simulations started Jan 2025 for a one year spin up and lasted till the Dec 2035. The ocean boundary conditions sea surface temperature and sea ice coverage were taken from coupled ECHAM5-OM simulations of the A1B scenario for the 4th IPCC report. Natural emissions of dust, (dry) salt, dimethyl sulfide (DMS) are deduced from the calculated wind fields. Continuous and explosive volcanic SO2 emissions and organic matter (SOA) emissions are prescribed by constant input files. For the biomass burning emissions, inventory files for the years 1997-2002 were cyclically used. For details: (Stier et al., 2005). The anthropogenic emissions of organic carbon (OC), black carbon (BC), and SO2 were taken from the ACCMIP RCP 8.5 scenario (Riahi et al., 2007), more precisely the linear interpolations between the given decadal values. In the reference run all emissions were kept as given, in the "MC off" scenario, all anthropogenic "Megacity" emissions were switched off. As any city borders are not known for the future, the predicted population density (by Vadim Chirkov, IIASA) for the year 2030 on a 0.5°× 0.5° grid was used. Every grid cell with a population density above 150 inhabitants per km2 was assigned to be a "megacity grid cell", see **Fehler! Verweisquelle konnte nicht gefunden werden.**. The anthropogenic emissions in these grid cells in the ACCMIP.8.5 files with 0.5°× 0.5° resolution were set to zero and after that, the emission files were interpolated to the T63 model resolution.

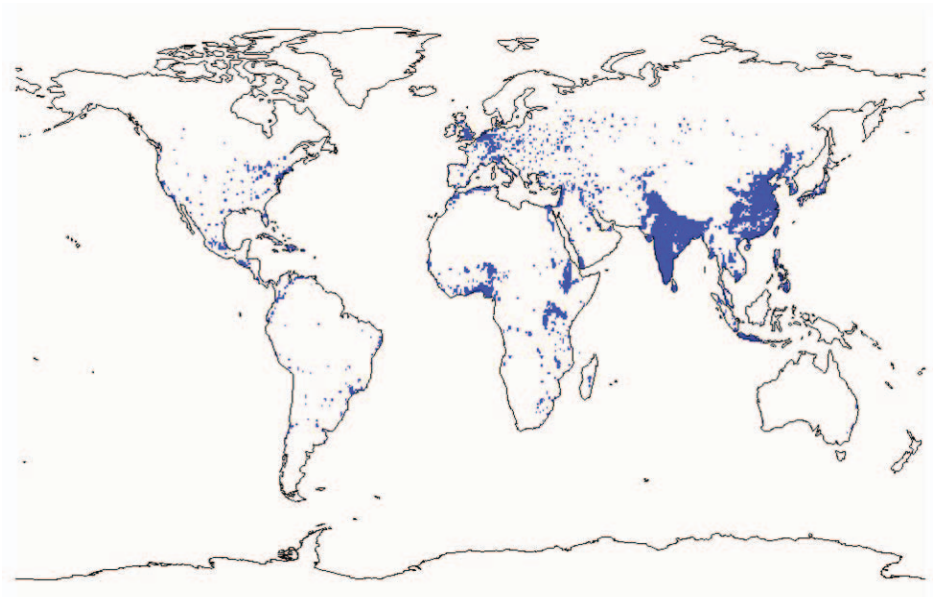

Figure 14 "Megacity" mask for the year 2030 used for switching of anthropogenic megacity emissions in the ACCMIP RCP 8.5 emission files. In the 0.5°□ 0.5° grid cells a threshold of 150 inhabitants per km2 was used.

2.6.2 Results

As shown above ECHAM5 does a quite good job in predicting mean values but doesn't perform very well concerning variability or trends, if the modelling period is to short and the ensemble to small. As the modelling period is even shorter this time (only ten years instead of 20) and no ensembles but only a single run has been performed for the reference and the "MC off" scenario, respectively, we will only look at decadal mean values in the following.

Figure 15 displays the top of the atmosphere (TOA) and surface (SUR) direct aerosol radiative forcing from the base case simulation. As explained in IPCC, 2007, aerosols with some absorbing component lead to negative TOA forcing over dark surfaces (e.g. oceans), while they can exhibit slightly positive TOA forcing over bright surfaces. The minimum forcing is -20 W m^{-2} over the tropical Atlantic while the maximum (positive) forcing is +5.3 W m^{-2} over the Sahara. Aerosols always cool the surface (Figure 15 right panel). The minimum SUR forcing is -32.5 W m^{-2}.

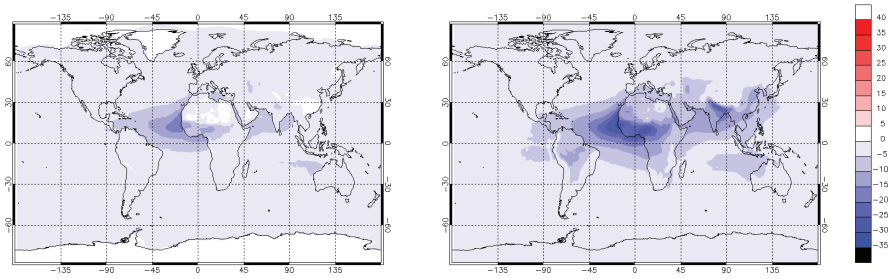

Figure 11 Instantaneous direct radiative forcing due to aerosols at the top of the atmosphere (left) and at the surface (right). Shown here are deacadal annual mean values from the base case simulation. [Units: W m^{-2}]

Figure 16 shows the total radiative forcing difference between the "MC on" and "MC off" simulations and thus gives an indication about the importance of megacity aerosol emissions on the climate system. Net reductions of the surface shortwave irradiance of up to -23 Wm^{-2} are found over the Ganges region and over China. At the top of the atmosphere, megacity emissions exert a much smaller influence which is predominantly positive (up to +3.1 W m^{-2} over China).Of the other world regions with megacity emissions, only Africa yields a noticeable impact on the radiative balance. Here, TOA forcing is enhanced by up to 1 W m^{-2} while surface radiation is reduced by up to -3.1 Wm-2. The radiative forcing changes for Europe are shown in Figure 17. The small signal of megacity emission in Europe leads to a slight cooling effect over western Europe and the North Atlantic while it exacerbates warming in the Mediterranean region. Note that the simulation does include indirect aerosol effects so that this net radiation change includes the changes in cloud properties which are further analyzed below.

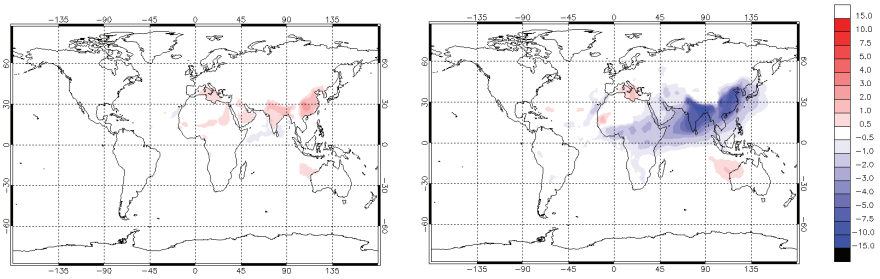

Figure 12 Effect of megacity emissions (see Figure 10) on the instantaneous direct aerosol radiative forcing at the top of the atmosphere (left) and at the surface (right). The figures display the "MC on" minus "MC off" results. [Units: W m^{-2}]

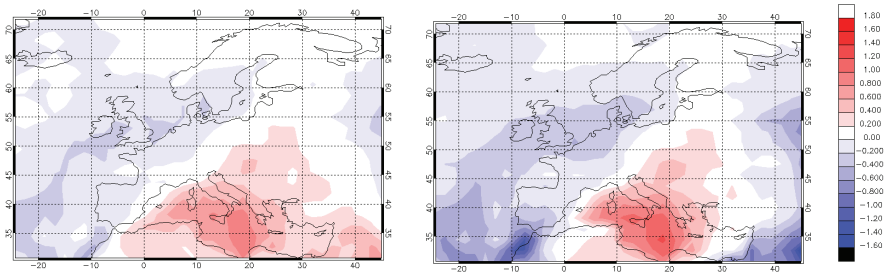

Figure 13 Same as Figure 14, but for Europe only. Note the different color scale. [Units: W m^{-2}]

In the table below we list the global average aerosol radiative forcing terms from the reference and sensitivity simulation, respectively. As discussed above the megacity emissions induce additional cooling at the surface. The signal at the top of the atmosphere is less clear because the clear sky radiative forcing calculation yields a small cooling effect while the all-sky calculation (including clouds) exhibits a small warming effect.

Table 3 Global mean and decadal mean aerosol forcing terms of the MC on and MC off simulations, respectively

	MC off	MC on
Shortwave clear sky forcing TOA [W m^{-2}]	-4.13	-4.16
Shortwave total forcing TOA [W m^{-2}]	-2.42	-2.38
Shortwave clear sky forcing SUR [W m^{-2}]	-5.81	-6.22
Shortwave total sky forcing SUR [W m^{-2}]	-3.94	-4.25
Longwave clear sky forcing TOA [W m^{-2}]	0.37	0.37
Longwave total forcing TOA [W m^{-2}]	0.22	0.22
Longwave clear sky forcing SUR [W m^{-2}]	1.62	1.62
Longwave total sky forcing SUR [W m^{-2}]	1.03	1.03

The aerosol emissions from megacities tend to increase large-scale precipitation in large regions of the tropical and subtropical belt, while they reduce precipitation in some areas of the North Pacific and the Indian Ocean as shown in Figure 18. Due to the short episode

of the simulation and the lack of ensemble simulations, these results should be treated with care as they are not statistically robust.

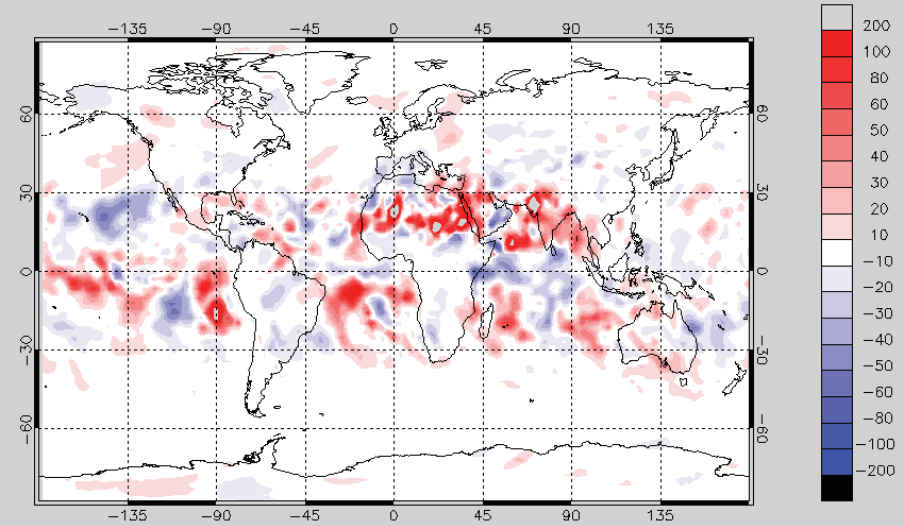

Figure 14 Relative changes (in %) in large-scale precipitation due to megacity aerosol emissions.

Humidity changes due to megacity emissions are shown in Figure 19. While the atmospheric water content near the surface tends to decrease over large parts of the northern mid latitudes with megacity aerosol emissions turned on, India and Australia would experience somewhat more humid air according to these simulations. In the middle troposphere the megacity aerosols generally tend to reduce humidity.

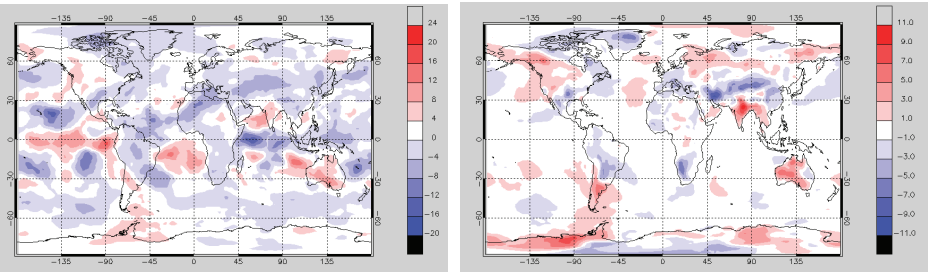

Figure 15 Relative changes (in %) in atmospheric water content at 450 hPa (left) and at the surface (right) due to megacity aerosol emissions.

Figure 16 displays the cloud droplet number concentration of the reference and sensitivity run, respectively. This exhibits an enormous increase in the CDNC concentration over China due to the aerosol emissions in this region. Elsewhere, the signal is much weaker and statistically less reliable. Figure 21 shows the change in the CDNC concentration over Europe. A significant increase of CDNC at the surface can be seen for England and the BENELUX region. This is consistent with the megacity emissions from these regions (see Figure 14). However, large increases are also found elsewhere in regions which are not directly influenced by such emissions.

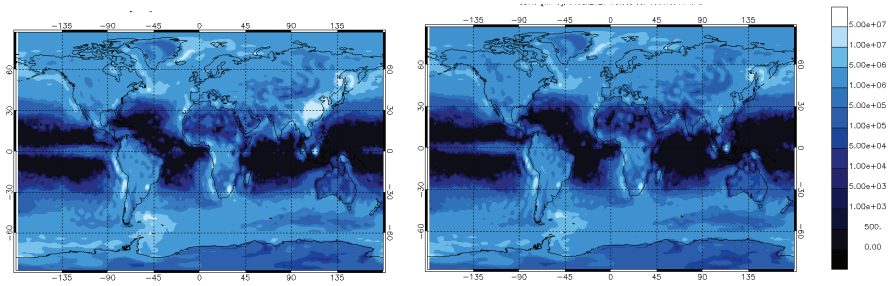

Figure 16 Cloud droplet number concentration at the surface of the reference simulation (left) and the "MC off" run (right). [Units: m-3]

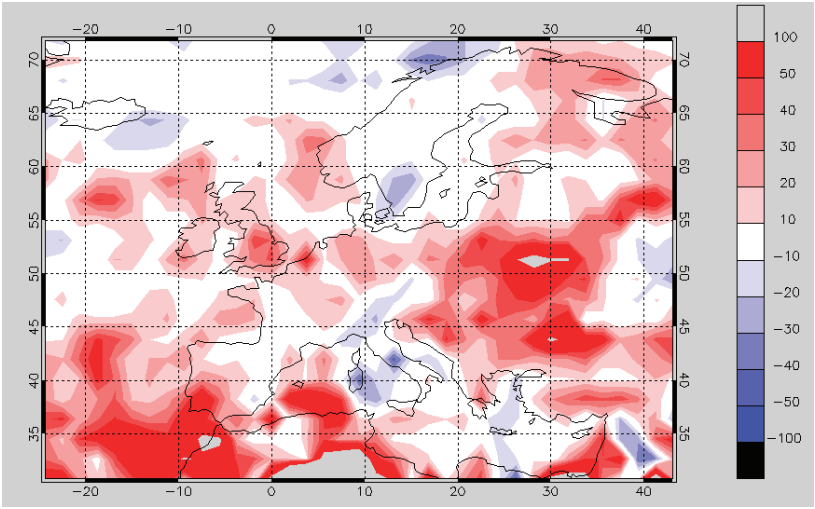

Figure 17 Change in the cloud droplet number concentration at the surface over Europe due to the influence of megacity emissions. [Units: %]

2.7 Conclusions

Two long-term sensitivity simulations were carried out using a chemistry and an aerosol package for the general circulation model ECHAM5, respectively, in order to assess the impact of meteorological variability on surface ozone concentrations over Europe and the impact of aerosol megacity emissions on the radiative budget of the atmosphere and on cloud properties.

The tropospheric gas-phase chemistry simulations with ECHAM5-MOZ were analyzed with respect to their mean values during the 1990-2008 period and with respect to the variability of surface temperatures and surface ozone concentrations. One simulation with meteorological analyses from the ECMWF ERA-Interim reanalysis was compared to another run which only used prescribed sea surface temperature and sea ice fields. Both runs yielded rather similar mean temperature and ozone distributions, but the variability of

summertime ozone concentrations over Eastern Europe was much smaller in the unnudged simulation than in the run with ERA-Interim meteorology. Interestingly, the 5% and 95%-iles of temperature and ozone during the 1990s were rather similar between the two runs. This leads us to conclude that the differences occurred after 2000 (when meteorological fields were taken from operational ECMWF analyses and more extreme summer heat conditions were encountered in Europe). Further analysis is required to confirm this hypothesis. Ozone trend analysis from both simulations shows practically no change over most of Europe while surface ozone increased over the Mediterranean. The unnudged simulation also yields a significant trend over the Iberian Peninsula and in Eastern Europe, which is absent from the nudged run.

For the analysis of climate impacts of megacity emissions we chose to perform two future scenario simulations around the year 2030 based on the ACCMIP RCP8.5 emission scenario. One simulation (reference) used all emissions, while in the other run, all aerosol emissions from "megacity grid boxes" (population density > 150 km^{-2}) were switched off. While this set-up doesn't necessarily provide a realistic description of future megacity emissions, it serves to (i) highlight the major impact regions and (ii) induces signals that are large enough to find statistically robust perturbations. The surface radiative forcing due to megacity aerosol emissions was found to be up to -32 Wm^{-2} while the combination of direct and indirect aerosol effects leads to a slight warming at the top of the atmosphere. Cloud condensation nuclei are generally enhanced due to the megacity contributions and this can be seen even in Europe where the perturbation is relatively small. While this provides a first cursory assessment of the potential impacts of large anthropogenic aerosol sources, more simulations and analyses will be necessary in order to accurately quantify the megacity impacts on climate. Changes in cloud properties in the vicinity of large agglomerations can change weather patterns and therefore influence cloud properties in other regions and it is therefore difficult to disentangle the effect of a specific megacity region in the simulations we have performed for CityZen.

2.8 Acknowledgements

The authors thank the Jülich Supercomputing Centre for providing the computational resources necessary to carry out the simulations described in this report. C. Richter acknowledges funding from the European Union under the CityZen project (grant 212095). Technical help by S. Schröder and various other colleagues was greatly appreciated.

2.9 References

A. M. Aghedo, S. Rast and M. G. Schultz (2010). "Sensitivity of tracer transport to model resolu-tion, prescribed meteorology and tracer lifetime in the general circulation model ECHAM5." At-mos. Chem. Phys. 10(7): 3385-3396.

R. Alley, T. Berntsen, N. L. Bindoff, Z. Chen, A. Chidthaisong, P. Friedlingstein, J. Gregory, G. Hegerl, M. Heimann, B. Hewitson, B. Hoskins, F. Joos, J. Jouzel, V. Kattsov, U. Lohmann, M. Manning, T. Matsuno, M. Molina, N. Nicholls, J. Overpeck, D. Qin, G. Raga, V. Ramaswamy, J. Ren, M. Rusticucci, S. Solomon, R. Somerville, T. F. Stocker, P. Stott, R. J. Stouffer, P. Whetton, R. A. Wood and D. Wratt (2007). Climate Change 2007: The Physical Science Basis, Summary for Policymakers. Geneva, Switzerland, Intergovernmetal Panel on Climate Change (WMO, UNEP): 1-21.

P. Bergamaschi, C. Frankenberg, J. F. Meirink, M. Krol, M. G. Villani, S. Houweling, F. Dentener, E. J. Dlugokencky, J. B. Miller, L. V. Gatti, A. Engel and I. Levin (2009). "Inverse modeling of global and regional CH4 emissions using SCIAMACHY satellite retrievals." J. Geophys. Res. 114.

G. P. Brasseur, X. Tie, P. J. Rasch and F. Lefèvre (1997). "A three-dimensional simulation of the Antarctic ozone hole: Impact of anthropogenic chlorine on the lower stratosphere and upper tropo-sphere." J. Geophys. Res. 102(D7): 8909-8930.

S. Deely, D. Dodman, J. Hardoy, C. Johnson, D. Satterthwaite, A. Serafin and R. Waddington (2010). World Disaster Report 2010 - Focus on urban risk. Geneva, Switzerland, International Fed-eration of Red Cross and Red Crescent Societies.

G. Dyner (2008). Climate Wars. Toronto, Canada, Random House of Canada.

A. M. Fiore, F. J. Dentener, O. Wild, C. Cuvelier, M. G. Schultz, P. Hess, C. Textor, M. Schulz, R. M. Doherty, L. W. Horowitz, I. A. MacKenzie, M. G. Sanderson, D. T. Shindell, D. S. Stevenson, S. Szopa, R. Van Dingenen, G. Zeng, C. Atherton, D. Bergmann, I. Bey, G. Carmichael, W. J. Col-lins, B. N. Duncan, G. Faluvegi, G. Folberth, M. Gauss, S. Gong, D. Hauglustaine, T. Holloway, I. S. A. Isaksen, D. J. Jacob, J. E. Jonson, J. W. Kaminski, T. J. Keating, A. Lupu, E. Marmer, V. Montanaro, R. J. Park, G. Pitari, K. J. Pringle, J. A. Pyle, S. Schroeder, M. G. Vivanco, P. Wind, G. Wojcik, S. Wu, and A. Zuber (2009), Multi-model Estimates of Intercontinental Source-Receptor Relationships for Ozone Pollution, J. Geophys. Res. 114, D04301, doi:10.1029/2008JD010816.

L. Ganzeveld and J. Lelieveld (1995). "Dry deposition parameterization in a chemistry general cir-culation model and its influence on the distribution of reactive trace gases." Journal of Geophysical Research 100: 20999-21012.

V. Grewe, D. Brunner, M. Dameris, J. L. Grenfell, R. Hein, D. Shindell and J. Staehelin (2001). "Origin and variability of upper tropospheric nitrogen oxides and ozone at northern mid-latitudes." Atmospheric Environment 35(20): 3421-3433.

A. Guenther, T. Karl, P. Harley, C. Wiedinmyer, P. I. Palmer and C. Geron (2006). "Estimates of global terrestrial isoprene emissions using MEGAN (Model of Emissions of Gases and Aerosols from Nature)." Atmos. Chem. Phys. J1 - ACP 6(11): 3181-3210.

Ø. Hodnebrog, F. Stordal and T. K. Berntsen (2011). "Does the resolution of megacity emissions impact large scale ozone?" Atmospheric Environment available online 14 January 2011.

L. W. Horowitz, S. Walters, D. L. Mauzerall, L. K. Emmons, P. J. Rasch, C. Granier, X. Tie, J.-F. Lamarque, M. G. Schultz, G. S. Tyndall, J. J. Orlando and G. P. Brasseur (2003). "A global simula-tion of tropospheric ozone and related tracers: Description and evaluation of {MOZART}, version 2." Journal of Geophysical Research 108(D24): 4784.

J. W. Hurrell, J. J. Hack, D. Shea, J. M. Caron and J. Rosinski (2008). "A New Sea Surface Tem-perature and Sea Ice Boundary Dataset for the Community Atmosphere Model." Journal of Climate 21(19): 5145-5153.

M. Koçak, C. Theodosi, P. Zarmpas, U. Im, A. Bougiatioti, O. Yenigun and N. Mihalopoulos (2010). "Particulate matter (PM10) in Istanbul: Origin, source areas and potential impact on sur-rounding regions." Atmospheric Environment available online 15 October 2010.

J. F. Lamarque, T. C. Bond, V. Eyring, C. Granier, A. Heil, Z. Klimont, D. Lee, C. Liousse, A. Mieville, B. Owen, M. G. Schultz, D. Shindell, S. J. Smith, E. Stehfest, J. Van Aardenne, O. R. Cooper, M. Kainuma, N. Mahowald, J. R. McConnell, V. Naik, K. Riahi and D. P. van Vuuren (2010). "Historical (1850-2000) gridded anthropogenic and biomass burning emissions of reactive gases and aerosols: methodology and application." Atmos. Chem. Phys. 10(15): 7017-7039.

T. Leisner (2005). Aerosols and their Role in the Atmosphere. WE-Heraeus-Summerschool "Phys-ics of the Environment"

S.-J. Lin and R. B. Rood (1996). "Multidimensional Flux-Form Semi-Lagrangian Transport Schemes." Monthly Weather Review: 2046-2070.

J. A. Logan (1999). "An analysis of ozonesonde data for the troposphere: Recommendations for testing 3-D models and development of a gridded climatology for tropospheric ozone." J. Geophys. Res. 104(D13): 16115-16149.

S. Madronich and S. Flocke (1999). The role of solar radiation in atmospheric chemistry. Handbook of Environmental Chemistry, Environmental Photochemistry. P. Boule, Springer Verlag.

T. E. Nordeng (1994). "Extended versions of the convective parameterization scheme at {ECMWF} and their impact on the mean transient activity of the model in the tropics." ECMWF Technical Memorandum 206.

H. Price, L. Jaeglé, A. Rice, P. Quay, P. C. Novelli and R. Gammon (2007). "Global budget of mo-lecular hydrogen and its deuterium content: Constraints from ground station, cruise, and aircraft observations." Journal of geophysical research 112(D22).

W. J. Randel, F. Wu, J. M. Russell, A. Roche and J. W. Waters (1998). "Seasonal Cycles and QBO Variations in Stratospheric CH4 and H2O Observed in UARS HALOE Data." Journal of the At-mospheric Sciences 55(2): 163-185.

K. Riahi, A. Grübler and N. Nakicenovic (2007). "Scenarios of long-term socio-economic and envi-ronmental development under climate stabilization." Technological Forecasting and Social Change 74(7): 887-935.

C. Richter (2008). Ozone Production in the Atmosphere Simulation Chamber SAPHIR. Jülich, For-schungszentrum Jülich GmbH, Zentralbibliothek, Verlag.

E. Roeckner, G. Bäuml, L. Bonaventura, R. Brokopf, M. Esch, M. Giorgetta, S. Hagemann, I. Kirchner, L. Kornblueh, E. Manzini, A. Rhodin, U. Schlese, U. Schulzweida and A. Tompkins (2003). the atmospheric general circulation model ECHAM5, part I. Hamburg, Max Planck Institute for Meteorology.

E. Roeckner, R. Brokopf, M. Esch, M. Giorgetta, S. Hagemann, L. Kornblueh, E. Manzini, U. Schlese and U. Schulzweida (2006). "Sensitivity of Simulated Climate to Horizontal and Vertical Resolution in the ECHAM5 Atmosphere Model." Journal of Climate 19(16): 3771-3791.

J. H. Seinfeld and S. N. Pandis (1998). Atmospheric Chemistry and Physics: From Air pollution to Climate change, John Wiley, United States of America.

P. Stier, J. Feichter, S. Kinne, S. Kloster, E. Vignati, J. Wilson, L. Ganzeveld, I. Tegen, M. Werner, Y. Balkanski, M. Schulz, O. Boucher, A. Minikin and A. Petzold (2005). "The aerosol-climate model ECHAM5-HAM." Atmos. Chem. Phys. 5(4): 1125-1156.

M. Tiedtke (1989). "A Comprehensive Mass Flux Scheme for Cumulus Parameterization in Large-Scale Models." Monthly Weather Review: 1779-1800.

3 Implications for mitigation strategies on air pollution under climate change

Frode Stordal and Øivind Hodnebrog, University of Oslo, Norway

3.1 Abstract

We have first estimated the impact of climate change on the chemical composition of the troposphere due to changes in climate from current climate (2000-2010) looking 40 years ahead (2040-2050), and next investigated the impact of mitigation of emissions of ozone precursors for ozone formation under current as well as future climate. The climate projection has been made by the ECHAM5 model and was followed by chemistry-transport modelling using a global model, Oslo CTM2 (Isaksen et al., 2005; Søvde et al., 2008). In this report we focus on carbon monoxide (CO) and surface ozone (O_3) which are measures of primary and secondary air pollution.

3.2 Changes in climate from 2000-2010 to 2040-2050 predicted by ECHAM5

ECHAM5 has been run for this study in CityZen from year 2000 to year 2050. It was run using precalculated sea surface temperatures (SST) from a coupled climate model run with ECHAM5/MPIOM from the IPCC AR4 assuming emissions of greenhouse gases and aerosols according to scenario A1B (Nakicenovic et al., 2000). The A1 storyline and scenario family describes a future world of very rapid economic growth, global population that peaks in mid-century and declines thereafter, and the rapid introduction of new and more efficient technologies. Major underlying themes are convergence among regions, capacity building and increased cultural and social interactions, with a substantial reduction in regional differences in per capita income. The A1 scenario family develops into three groups that describe alternative directions of technological change in the energy system, where A1B assumes a balance across all energy sources. The change in climate parameters has been reviewed in Deliverable Report 2.3.1 and is only briefly mentioned here. Temperatures increase in the 40 year period from 2000-2010 to 2040-2050 in the troposphere and decrease in the stratosphere, in agreement with known impacts of greenhouse gases. The warming, in Northern Hemisphere summer, was in general larger over continents than oceans, and with marked warming at high latitudes. There are also regions with cooling, most noticeably over the North Atlantic Ocean. In parts of Europe and China regional cooling from aerosols is evident, opposing the large scale warming due to the greenhouse gases. As expected, a warmer troposphere in 2040-2050 has a higher specific moisture. The pattern of moistening to a large extent follows the pattern of warming, so that e.g. Europe will gain less. Other parameters in the water cycle that impact the atmospheric chemistry are precipitation and cloud cover, regulating wet deposition of water soluble chemical species and thus radiative transfer and photo-dissociation rates respectively. Changes in these two parameters are clearly related to atmospheric moisture and also to each other. At low and mid latitudes, the fraction of mid and high level clouds decreases, whereas there is an increase in the fraction of low level clouds. The low level clouds increase their fraction in parts of Europe, whereas they decrease their fraction in other parts. Over India there is a noticeable decrease in precipitation

as well as in cloud fraction. In China precipitation increases in the central and southern parts, whereas there is a drying in the north. Low level clouds follow the same pattern, with increased cloudiness in the south and decreased in the north.

3.3 Emission scenarios for 2050

We have estimated the changes in chemistry due to changes in anthropogenic emissions, adopting two scenarios where certain mitigation measures represent the only difference. We have selected the HIGH-CLE and the HIGH-FROZEN scenarios developed by IIASA for this purpose. The HIGH-FROZEN scenario assumes that there is no change in future pollution policies relative to 2005. The combustion technologies/abatement measures are assumed not to change beyond the year 2005 technologies for the entire period 2000-2050. While for OECD countries, this implies a continuation of current high levels of control, for many developing countries where air quality legislation are only very recently becoming implemented, this could mean a continuation of low legislation levels as in the past. There is also no implementation of policies on energy access, although increasing economic growth leads to a slowly declining use of dirty solid fuels for cooking and heating in developing regions. As a result pollution levels in this scenario are the highest among the scenarios described.

The HIGH-CLE scenario is identical to the case described above in terms of energy structure and no specific policies on climate change and energy access. However, it assumes full implementation of all current and planned air pollution legislation world-wide until 2030. Thus this scenario provides a measure of the impact of current and planned air pollution policies in the absence of any specific climate or energy access policy.

The anthropogenic emissions of CO and NOx in the two scenarios are shown in Figures 1 and 2 along with the difference between the two. We see that in Europe emission legislation will result in reductions in emissions of CO as well as NOx in the mitigation case. All across Europe CO (Figure 1) and NOx (Figure 2) emissions are lower in HIGH-CLE than in HIGH-FROZEN. Naturally, this is the case all over the globe. In absolute terms, the difference between the two, and thus the impact of mitigation, is largest in Asia, most notably in large parts of India and China where the emissions before mitigation are clearly highest.

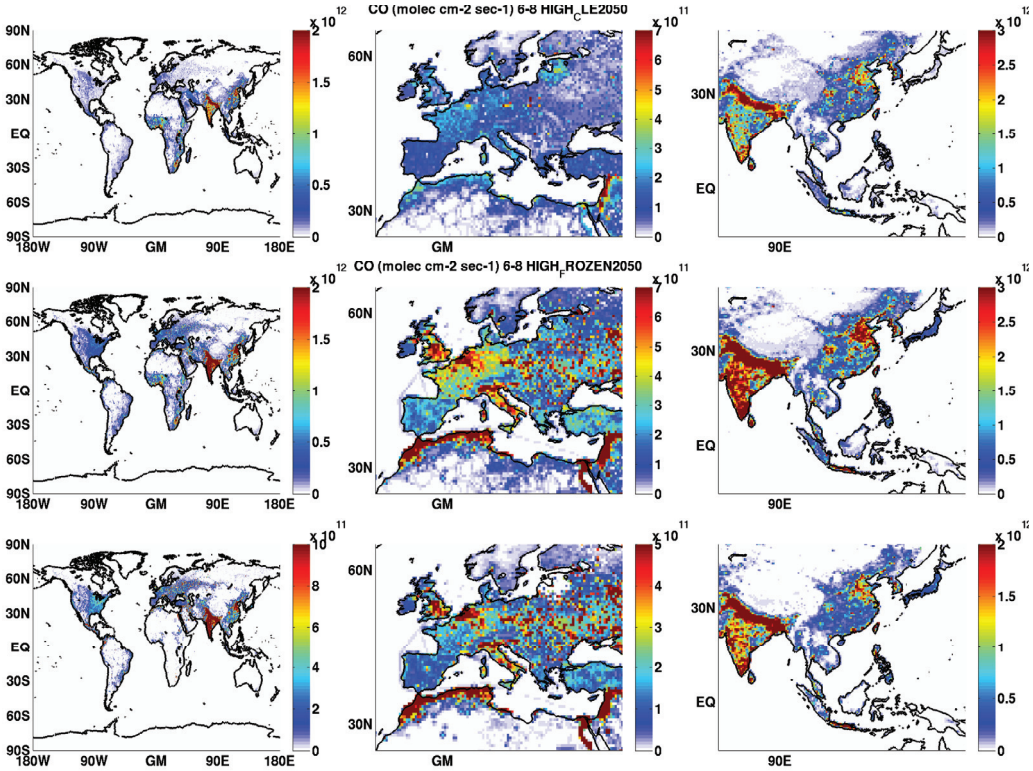

Figure 1: Anthropogenic emissions of CO (molec cm^{-2} s^{-1}) in the period June-August for the 2050 HIGH CLE (top) and HIGH FROZEN (middle) scenarios, and as differences between the two scenarios (bottom). Note that the scales are different.

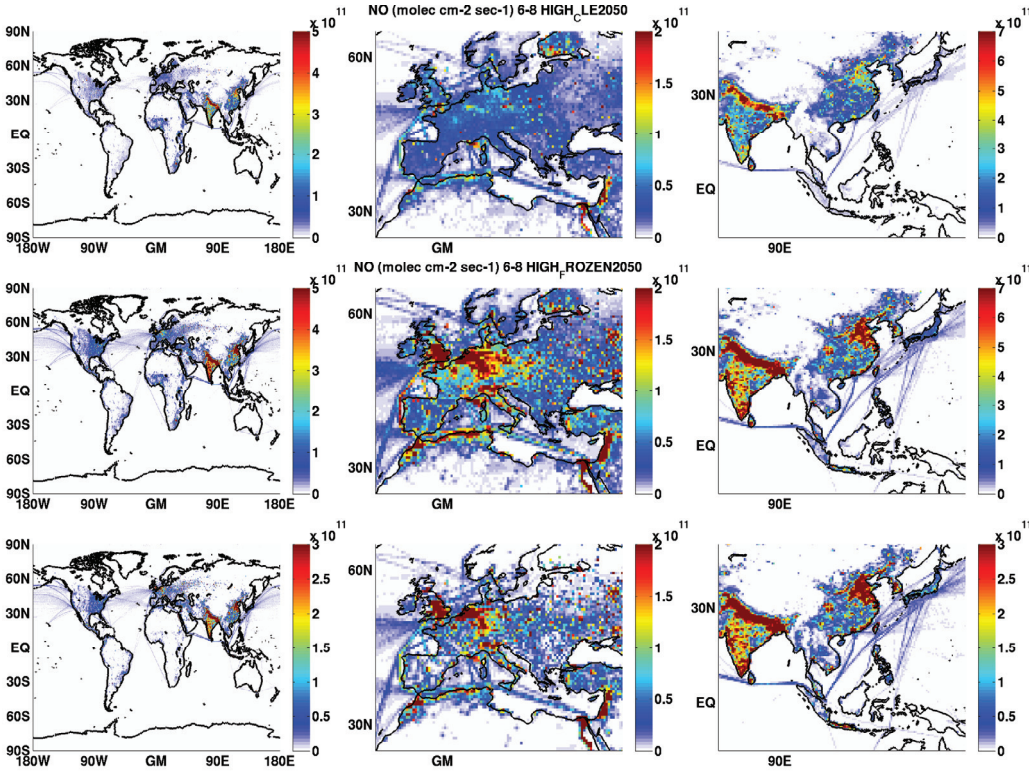

Figure 2: Anthropogenic emissions of NO_X (molec cm^{-2} s^{-1}) in the period June-August for the 2050 HIGH CLE (top) and HIGH FROZEN (middle) scenarios, and as differences between the two scenarios (bottom). Note that the scales are different.

3.4 Implications for mitigation strategies on near-surface CO predicted by the OsloCTM2

CO concentrations resulting from anthropogenic emissions retain a pattern which is similar to the emission pattern, although somewhat smeared out due to transport of CO some distance away from the sources (Figure 3). Mitigation of CO emissions is seen most clearly over the UK, in Central Europe and in the Mediterranean region along the southern and eastern boundaries of the Mediterranean Sea. However, it is worth noticing that the effects of mitigation on the CO distribution in much of Europe is only moderately impacted by the change in meteorology due to climate change from 2000-2010 to 2040-2050 (Figure 3). Over the Mediterranean region the impact exceeds 15 µg m^{-3} in certain areas, which is not negligible. The same size impact is seen over larger parts of India, where climate change is rather important for the atmospheric chemistry. Over China the impact is somewhat weaker but very wide spread, up to about 5 µg m^{-3}.

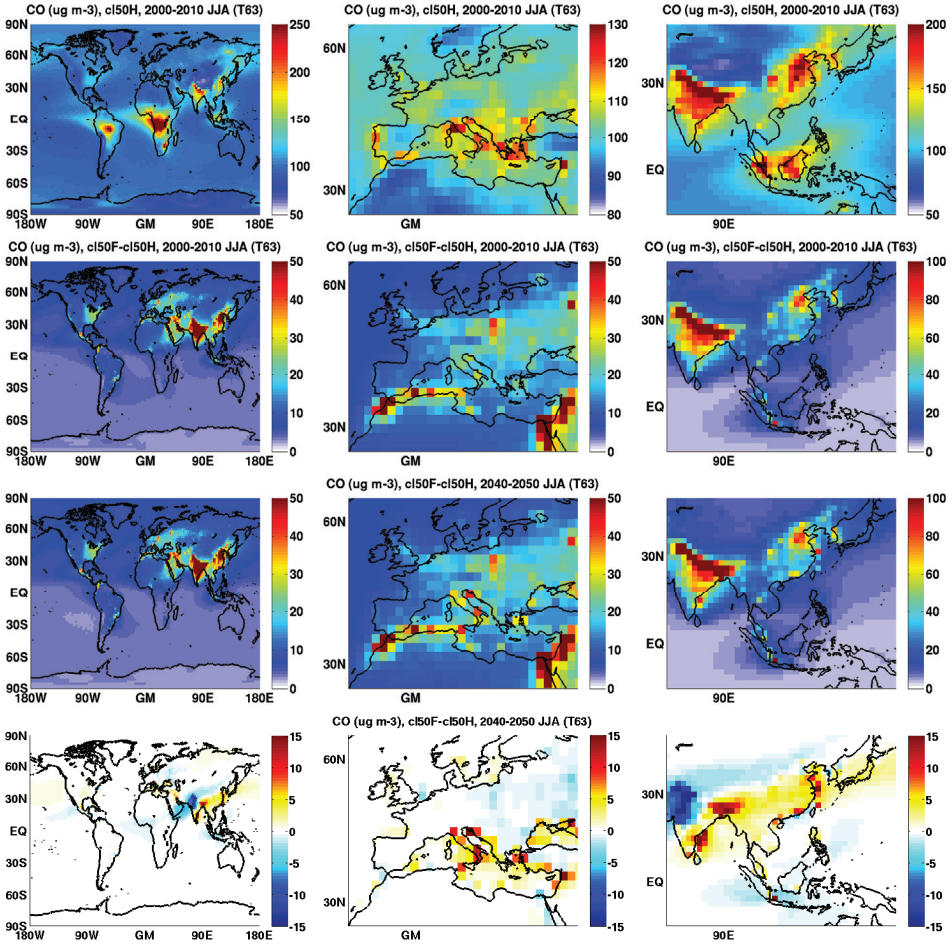

Figure 3: 11-year average of near-surface CO (µg m^{-3}) for the northern hemisphere summer (June, July, August) shown (i) for the simulations with current climate (2000-2010) and 2050 HIGH CLE emissions (top), (ii) as difference between simulations with 2050 HIGH FROZEN and 2050 HIGH CLE emissions (2nd row), (iii) for future climate as difference between simulations with 2050 HIGH FROZEN and 2050 HIGH CLE emissions (3rd row), and (iv) for differences between the two latter cases (ii and iii; bottom row). Note that the scales are different.

3.5 Implications for mitigation strategies on daily max. near-surface ozone predicted by the Oslo CTM2 model

Ozone concentrations resulting from anthropogenic emissions are impacted by emissions of all the ozone precursors, thus following the emission patterns of both CO and NOx as shown in Figures 1 and 2. Mitigation of ozone precursor emissions are seen most clearly over the Mediterranean region, but also in Central Europe. However, as for CO, it is worth noticing that the effects of mitigation on the ozone distribution in Europe is only modestly impacted by the change in meteorology due to climate change from 2000-2010 to 2040-2050 (Figure 4), even though the impact is slightly stronger than for CO. The geographical distribution across Europe is roughly like the one for CO, and the largest impacts exceed 10 μg m^{-3} or 5 ppb. A similar effect is seen over much of India, where climate change is rather important for the atmospheric chemistry. All in all, the conclusion of this work, given the climate scenario and emission scenarios that we have adopted, is that the climate change impacts results of mitigation of ozone precursor emissions on air pollution are relatively moderate, but clearly not negligible. Thus mitigation strategies may not need to be drastically altered. However, the effects are large enough to call for further investigation, including also other climate change and emission scenarios.

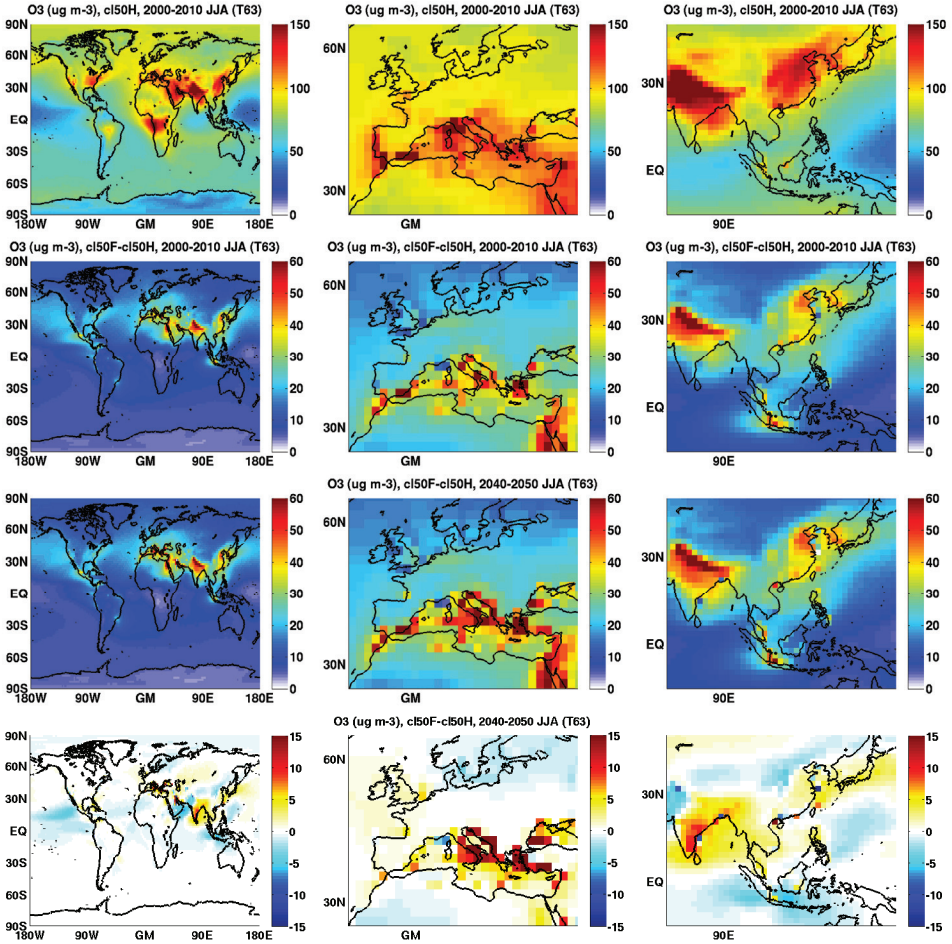

Figure 4: Same as Figure 3, except average of daily max near-surface ozone.

3.6 References

Isaksen, I. S. A., Zerefos, C., Kourtidis, K., Meleti, C., Dalsoren, S. B., Sundet, J. K., Grini, A., Zanis, P., and Balis, D.: Tropospheric ozone changes at unpolluted and semipolluted regions induced by stratospheric ozone changes, J. Geophys. Res.-Atmos., 110 (D2), 10.1029/2004jd004618, 2005.

Nakicenovic, N., Davidson, O., Davis, G., Grübler, A., Kram, T., La Rovere, E. L., Metz, B., Morita, T., Pepper, W., Pitcher, H., Sankovski, A., Shukla, P., Swart, R., Watson, R., and Dadi, Z.: Special Report on Emissions Scenarios, Cambridge University Press, Cambridge, 599 pp, 2000.

Søvde, O. A., Gauss, M., Smyshlyaev, S. P., and Isaksen, I. S. A.: Evaluation of the chemical transport model Oslo CTM2 with focus on arctic winter ozone depletion, J. Geophys. Res.-Atmos., 113 (D9), 10.1029/2007jd009240, 2008.

1. **Einsatz von multispektralen Satellitenbilddaten in der Wasserhaushalts- und Stoffstrommodellierung – dargestellt am Beispiel des Rureinzugsgebietes**
   von C. Montzka (2008), XX, 238 Seiten
   ISBN: 978-3-89336-508-1

2. **Ozone Production in the Atmosphere Simulation Chamber SAPHIR**
   by C. A. Richter (2008), XIV, 147 pages
   ISBN: 978-3-89336-513-5

3. **Entwicklung neuer Schutz- und Kontaktierungsschichten für Hochtemperatur-Brennstoffzellen**
   von T. Kiefer (2008), 138 Seiten
   ISBN: 978-3-89336-514-2

4. **Optimierung der Reflektivität keramischer Wärmedämmschichten aus Yttrium-teilstabilisiertem Zirkoniumdioxid für den Einsatz auf metallischen Komponenten in Gasturbinen**
   von A. Stuke (2008), X, 201 Seiten
   ISBN: 978-3-89336-515-9

5. **Lichtstreuende Oberflächen, Schichten und Schichtsysteme zur Verbesserung der Lichteinkopplung in Silizium-Dünnschichtsolarzellen**
   von M. Berginski (2008), XV, 171 Seiten
   ISBN: 978-3-89336-516-6

6. **Politikszenarien für den Klimaschutz IV – Szenarien bis 2030**
   hrsg.von P. Markewitz, F. Chr. Matthes (2008), 376 Seiten
   ISBN 978-3-89336-518-0

7. **Untersuchungen zum Verschmutzungsverhalten rheinischer Braunkohlen in Kohledampferzeugern**
   von A. Schlüter (2008), 164 Seiten
   ISBN 978-3-89336-524-1

8. **Inorganic Microporous Membranes for Gas Separation in Fossil Fuel Power Plants**
   by G. van der Donk (2008), VI, 120 pages
   ISBN: 978-3-89336-525-8

9. **Sinterung von Zirkoniumdioxid-Elektrolyten im Mehrlagenverbund der oxidkeramischen Brennstoffzelle (SOFC)**
   von R. Mücke (2008), VI, 165 Seiten
   ISBN: 978-3-89336-529-6

10. **Safety Considerations on Liquid Hydrogen**
    by K. Verfondern (2008), VIII, 167 pages
    ISBN: 978-3-89336-530-2

11. **Kerosinreformierung für Luftfahrtanwendungen**
von R. C. Samsun (2008), VII, 218 Seiten
ISBN: 978-3-89336-531-9

12. **Der 4. Deutsche Wasserstoff Congress 2008 – Tagungsband**
hrsg. von D. Stolten, B. Emonts, Th. Grube (2008), 269 Seiten
ISBN: 978-3-89336-533-3

13. **Organic matter in Late Devonian sediments as an indicator for environmental changes**
by M. Kloppisch (2008), XII, 188 pages
ISBN: 978-3-89336-534-0

14. **Entschwefelung von Mitteldestillaten für die Anwendung in mobilen Brennstoffzellen-Systemen**
von J. Latz (2008), XII, 215 Seiten
ISBN: 978-3-89336-535-7

15. **RED-IMPACT**
Impact of Partitioning, Transmutation and Waste Reduction Technologies on the Final Nuclear Waste Disposal
SYNTHESIS REPORT
ed. by W. von Lensa, R. Nabbi, M. Rossbach (2008), 178 pages
ISBN 978-3-89336-538-8

16. **Ferritic Steel Interconnectors and their Interactions with Ni Base Anodes in Solid Oxide Fuel Cells (SOFC)**
by J. H. Froitzheim (2008), 169 pages
ISBN: 978-3-89336-540-1

17. **Integrated Modelling of Nutrients in Selected River Basins of Turkey**
Results of a bilateral German-Turkish Research Project
project coord. M. Karpuzcu, F. Wendland (2008), XVI, 183 pages
ISBN: 978-3-89336-541-8

18. **Isotopengeochemische Studien zur klimatischen Ausprägung der Jüngeren Dryas in terrestrischen Archiven Eurasiens**
von J. Parplies (2008), XI, 155 Seiten, Anh.
ISBN: 978-3-89336-542-5

19. **Untersuchungen zur Klimavariabilität auf dem Tibetischen Plateau - Ein Beitrag auf der Basis stabiler Kohlenstoff- und Sauerstoffisotope in Jahrringen von Bäumen waldgrenznaher Standorte**
von J. Griessinger (2008), XIII, 172 Seiten
ISBN: 978-3-89336-544-9

20. **Neutron-Irradiation + Helium Hardening & Embrittlement Modeling of 9%Cr-Steels in an Engineering Perspective (HELENA)**
by R. Chaouadi (2008), VIII, 139 pages
ISBN: 978-3-89336-545-6

21. **in Bearbeitung**

22. **Verbundvorhaben APAWAGS (AOEV und Wassergenerierung) – Teilprojekt: Brennstoffreformierung – Schlussbericht**
von R. Peters, R. C. Samsun, J. Pasel, Z. Porš, D. Stolten (2008), VI, 106 Seiten
ISBN: 978-3-89336-547-0

23. **FREEVAL**
Evaluation of a Fire Radiative Power Product derived from Meteosat 8/9 and Identification of Operational User Needs
Final Report
project coord. M. Schultz, M. Wooster (2008), 139 pages
ISBN: 978-3-89336-549-4

24. **Untersuchungen zum Alkaliverhalten unter Oxycoal-Bedingungen**
von C. Weber (2008), VII, 143, XII Seiten
ISBN: 978-3-89336-551-7

25. **Grundlegende Untersuchungen zur Freisetzung von Spurstoffen, Heißgaschemie, Korrosionsbeständigkeit keramischer Werkstoffe und Alkalirückhaltung in der Druckkohlenstaubfeuerung**
von M. Müller (2008), 207 Seiten
ISBN: 978-3-89336-552-4

26. **Analytik von ozoninduzierten phenolischen Sekundärmetaboliten in *Nicotiana tabacum* L. cv Bel W3 mittels LC-MS**
von I. Koch (2008), III, V, 153 Seiten
ISBN 978-3-89336-553-1

27. **IEF-3 Report 2009. Grundlagenforschung für die Anwendung**
(2009), ca. 230 Seiten
ISBN: 978-3-89336-554-8

28. **Influence of Composition and Processing in the Oxidation Behavior of MCrAlY-Coatings for TBC Applications**
by J. Toscano (2009), 168 pages
ISBN: 978-3-89336-556-2

29. **Modellgestützte Analyse signifikanter Phosphorbelastungen in hessischen Oberflächengewässern aus diffusen und punktuellen Quellen**
von B. Tetzlaff (2009), 149 Seiten
ISBN: 978-3-89336-557-9

30. **Nickelreaktivlot / Oxidkeramik – Fügungen als elektrisch isolierende Dichtungskonzepte für Hochtemperatur-Brennstoffzellen-Stacks**
von S. Zügner (2009), 136 Seiten
ISBN: 978-3-89336-558-6

31. **Langzeitbeobachtung der Dosisbelastung der Bevölkerung in radioaktiv kontaminierten Gebieten Weißrusslands – Korma-Studie**
von H. Dederichs, J. Pillath, B. Heuel-Fabianek, P. Hill, R. Lennartz (2009), Getr. Pag.
ISBN: 978-3-89336-532-3

32. **Herstellung von Hochtemperatur-Brennstoffzellen über physikalische Gasphasenabscheidung**
von N. Jordán Escalona (2009), 148 Seiten
ISBN: 978-3-89336-532-3

33. **Real-time Digital Control of Plasma Position and Shape on the TEXTOR Tokamak**
by M. Mitri (2009), IV, 128 pages
ISBN: 978-3-89336-567-8

34. **Freisetzung und Einbindung von Alkalimetallverbindungen in kohlebefeuerten Kombikraftwerken**
von M. Müller (2009), 155 Seiten
ISBN: 978-3-89336-568-5

35. **Kosten von Brennstoffzellensystemen auf Massenbasis in Abhängigkeit von der Absatzmenge**
von J. Werhahn (2009), 242 Seiten
ISBN: 978-3-89336-569-2

36. **Einfluss von Reoxidationszyklen auf die Betriebsfestigkeit von anodengestützten Festoxid-Brennstoffzellen**
von M. Ettler (2009), 138 Seiten
ISBN: 978-3-89336-570-8

37. **Großflächige Plasmaabscheidung von mikrokristallinem Silizium für mikromorphe Dünnschichtsolarmodule**
von T. Kilper (2009), XVII, 154 Seiten
ISBN: 978-3-89336-572-2

38. **Generalized detailed balance theory of solar cells**
by T. Kirchartz (2009), IV, 198 pages
ISBN: 978-3-89336-573-9

39. **The Influence of the Dynamic Ergodic Divertor on the Radial Electric Field at the Tokamak TEXTOR**
von J. W. Coenen (2009), xii, 122, XXVI pages
ISBN: 978-3-89336-574-6

40. **Sicherheitstechnik im Wandel Nuklearer Systeme**
von K. Nünighoff (2009), viii, 215 Seiten
ISBN: 978-3-89336-578-4

41. **Pulvermetallurgie hochporöser NiTi-Legierungen für Implanat- und Dämpfungsanwendungen**
von M. Köhl (2009), XVII, 199 Seiten
ISBN: 978-3-89336-580-7

42. **Einfluss der Bondcoatzusammensetzung und Herstellungsparameter auf die Lebensdauer von Wärmedämmschichten bei zyklischer Temperaturbelastung**
von M. Subanovic (2009), 188, VI Seiten
ISBN: 978-3-89336-582-1

43. **Oxygen Permeation and Thermo-Chemical Stability of Oxygen Permeation Membrane Materials for the Oxyfuel Process**
by A. J. Ellett (2009), 176 pages
ISBN: 978-3-89336-581-4

44. **Korrosion von polykristallinem Aluminiumoxid (PCA) durch Metalljodidschmelzen sowie deren Benetzungseigenschaften**
von S. C. Fischer (2009), 148 Seiten
ISBN: 978-3-89336-584-5

45. **IEF-3 Report 2009. Basic Research for Applications**
(2009), 217 Seiten
ISBN: 978-3-89336-585-2

46. **Verbundvorhaben ELBASYS (Elektrische Basissysteme in einem CFK-Rumpf) - Teilprojekt: Brennstoffzellenabgase zur Tankinertisierung - Schlussbericht**
von R. Peters, J. Latz, J. Pasel, R. C. Samsun, D. Stolten
(2009), xi, 202 Seiten
ISBN: 978-3-89336-587-6

47. **Aging of ^{14}C-labeled Atrazine Residues in Soil: Location, Characterization and Biological Accessibility**
by N. D. Jablonowski (2009), IX, 104 pages
ISBN: 978-3-89336-588-3

48. **Entwicklung eines energetischen Sanierungsmodells für den europäischen Wohngebäudesektor unter dem Aspekt der Erstellung von Szenarien für Energie- und CO_2 - Einsparpotenziale bis 2030**
von P. Hansen (2009), XXII, 281 Seiten
ISBN: 978-3-89336-590-6

49. **Reduktion der Chromfreisetzung aus metallischen Interkonnektoren für Hochtemperaturbrennstofzellen durch Schutzschichtsysteme**
von R. Trebbels (2009), iii, 135 Seiten
ISBN: 978-3-89336-591-3

50. **Bruchmechanische Untersuchung von Metall / Keramik-Verbundsystemen für die Anwendung in der Hochtemperaturbrennstoffzelle**
von B. Kuhn (2009), 118 Seiten
ISBN: 978-3-89336-592-0

51. **Wasserstoff-Emissionen und ihre Auswirkungen auf den arktischen Ozonverlust**
Risikoanalyse einer globalen Wasserstoffwirtschaft
von T. Feck (2009), 180 Seiten
ISBN: 978-3-89336-593-7

52. **Development of a new Online Method for Compound Specific Measurements of Organic Aerosols**
by T. Hohaus (2009), 156 pages
ISBN: 978-3-89336-596-8

53. **Entwicklung einer FPGA basierten Ansteuerungselektronik für Justageeinheiten im Michelson Interferometer**
von H. Nöldgen (2009), 121 Seiten
ISBN: 978-3-89336-599-9

54. **Observation – and model – based study of the extratropical UT/LS**
by A. Kunz (2010), xii, 120, xii pages
ISBN: 978-3-89336-603-3

55. **Herstellung polykristalliner Szintillatoren für die Positronen-Emissions-Tomographie (PET)**
von S. K. Karim (2010), VIII, 154 Seiten
ISBN: 978-3-89336-610-1

56. **Kombination eines Gebäudekondensators mit H2-Rekombinatorelementen in Leichwasserreaktoren**
von S. Kelm (2010), vii, 119 Seiten
ISBN: 978-3-89336-611-8

57. **Plant Leaf Motion Estimation Using A 5D Affine Optical Flow Model**
by T. Schuchert (2010), X, 143 pages
ISBN: 978-3-89336-613-2

58. **Tracer-tracer relations as a tool for research on polar ozone loss**
by R. Müller (2010), 116 pages
ISBN: 978-3-89336-614-9

59. **Sorption of polycyclic aromatic hydrocarbon (PAH) to Yangtze River sediments and their components**
by J. Zhang (2010), X, 109 pages
ISBN: 978-3-89336-616-3

60. **Weltweite Innovationen bei der Entwicklung von CCS-Technologien und Möglichkeiten der Nutzung und des Recyclings von CO_2**
Studie im Auftrag des BMWi
von W. Kuckshinrichs et al. (2010), X, 139 Seiten
ISBN: 978-3-89336-617-0

61. **Herstellung und Charakterisierung von sauerstoffionenleitenden Dünnschichtmembranstrukturen**
von M. Betz (2010), XII, 112 Seiten
ISBN: 978-3-89336-618-7

62. **Politikszenarien für den Klimaschutz V – auf dem Weg zum Strukturwandel, Treibhausgas-Emissionsszenarien bis zum Jahr 2030**
hrsg. von P. Hansen, F. Chr. Matthes (2010), 276 Seiten
ISBN: 978-3-89336-619-4

63. **Charakterisierung Biogener Sekundärer Organischer Aerosole mit Statistischen Methoden**
von C. Spindler (2010), iv, 163 Seiten
ISBN: 978-3-89336-622-4

64. **Stabile Algorithmen für die Magnetotomographie an Brennstoffzellen**
von M. Wannert (2010), ix, 119 Seiten
ISBN: 978-3-89336-623-1

65. **Sauerstofftransport und Degradationsverhalten von Hochtemperaturmembranen für CO2-freie Kraftwerke**
von D. Schlehuber (2010), VII, 139 Seiten
ISBN: 978-3-89336-630-9

66. **Entwicklung und Herstellung von foliengegossenen, anodengestützten Festoxidbrennstoffzellen**
von W. Schafbauer (2010), VI, 164 Seiten
ISBN: 978-3-89336-631-6

67. **Disposal strategy of proton irradiated mercury from high power spallation sources**
by S. Chiriki (2010), xiv, 124 pages
ISBN: 978-3-89336-632-3

68. **Oxides with polyatomic anions considered as new electrolyte materials for solid oxide fuel cells (SOFCs)**
by O. H. Bin Hassan (2010), vii, 121 pages
ISBN: 978-3-89336-633-0

69. **Von der Komponente zum Stack: Entwicklung und Auslegung von HT-PEFC-Stacks der 5 kW-Klasse**
von A. Bendzulla (2010), IX, 203 Seiten
ISBN: 978-3-89336-634-7

70. **Satellitengestützte Schwerewellenmessungen in der Atmosphäre und Perspektiven einer zukünftigen ESA Mission (PREMIER)**
von S. Höfer (2010), 81 Seiten
ISBN: 978-3-89336-637-8

71. **Untersuchungen der Verhältnisse stabiler Kohlenstoffisotope in atmosphärisch relevanten VOC in Simulations- und Feldexperimenten**
von H. Spahn (2010), IV, 210 Seiten
ISBN: 978-3-89336-638-5

72. **Entwicklung und Charakterisierung eines metallischen Substrats für nanostrukturierte keramische Gastrennmembranen**
von K. Brands (2010), vii, 137 Seiten
ISBN: 978-3-89336-640-8

73. **Hybridisierung und Regelung eines mobilen Direktmethanol-Brennstoffzellen-Systems**
von J. Chr. Wilhelm (2010), 220 Seiten
ISBN: 978-3-89336-642-2

74. **Charakterisierung perowskitischer Hochtemperaturmembranen zur Sauerstoffbereitstellung für fossil gefeuerte Kraftwerksprozesse**
von S.A. Möbius (2010) III, 208 Seiten
ISBN: 978-3-89336-643-9

75. **Characterization of natural porous media by NMR and MRI techniques: High and low magnetic field studies for estimation of hydraulic properties**
by L.-R. Stingaciu (2010), 96 pages
ISBN: 978-3-89336-645-3

76. **Hydrological Characterization of a Forest Soil Using Electrical Resistivity Tomography**
by Chr. Oberdörster (2010), XXI, 151 pages
ISBN: 978-3-89336-647-7

77. **Ableitung von atomarem Sauerstoff und Wasserstoff aus Satellitendaten und deren Abhängigkeit vom solaren Zyklus**
von C. Lehmann (2010), 127 Seiten
ISBN: 978-3-89336-649-1

78. **18th World Hydrogen Energy Conference 2010 – WHEC2010 Proceedings**
Speeches and Plenary Talks
ed. by D. Stolten, B. Emonts (2010)
ISBN: 978-3-89336-658-3

78-1. **18th World Hydrogen Energy Conference 2010 – WHEC2010 Proceedings**
Parallel Sessions Book 1:
Fuel Cell Basics / Fuel Infrastructures
ed. by D. Stolten, T. Grube (2010), ca. 460 pages
ISBN: 978-3-89336-651-4

78-2. **18th World Hydrogen Energy Conference 2010 – WHEC2010 Proceedings**
Parallel Sessions Book 2:
Hydrogen Production Technologies – Part 1
ed. by D. Stolten, T. Grube (2010), ca. 400 pages
ISBN: 978-3-89336-652-1

78-3. **18th World Hydrogen Energy Conference 2010 – WHEC2010 Proceedings**
Parallel Sessions Book 3:
Hydrogen Production Technologies – Part 2
ed. by D. Stolten, T. Grube (2010), ca. 640 pages
ISBN: 978-3-89336-653-8

78-4. **18th World Hydrogen Energy Conference 2010 – WHEC2010 Proceedings**
Parallel Sessions Book 4:
Storage Systems / Policy Perspectives, Initiatives and Cooperations
ed. by D. Stolten, T. Grube (2010), ca. 500 pages
ISBN: 978-3-89336-654-5

78-5. **18th World Hydrogen Energy Conference 2010 – WHEC2010 Proceedings**
Parallel Sessions Book 5:
Stategic Analysis / Safety Issues / Existing and Emerging Markets
ed. by D. Stolten, T. Grube (2010), ca. 530 pages
ISBN: 978-3-89336-655-2

78-6. **18th World Hydrogen Energy Conference 2010 – WHEC2010 Proceedings**
Parallel Sessions Book 6:
Stationary Applications / Transportation Applications
ed. by D. Stolten, T. Grube (2010), ca. 330 pages
ISBN: 978-3-89336-656-9

78 Set (complete book series)

18th World Hydrogen Energy Conference 2010 – WHEC2010 Proceedings
ed. by D. Stolten, T. Grube, B. Emonts (2010)
ISBN: 978-3-89336-657-6

79. **Ultrafast voltex core dynamics investigated by finite-element micromagnetic simulations**
by S. Gliga (2010), vi, 144 pages
ISBN: 978-3-89336-660-6

80. **Herstellung und Charakterisierung von keramik- und metallgestützten Membranschichten für die CO_2-Abtrennung in fossilen Kraftwerken**
von F. Hauler (2010), XVIII, 178 Seiten
ISBN: 978-3-89336-662-0

81. **Experiments and numerical studies on transport of sulfadiazine in soil columns**
by M. Unold (2010), xvi, 115 pages
ISBN: 978-3-89336-663-7

82. **Prompt-Gamma-Neutronen-Aktivierungs-Analyse zur zerstörungsfreien Charakterisierung radioaktiver Abfälle**
von J.P.H. Kettler (2010), iv, 205 Seiten
ISBN: 978-3-89336-665-1

83. **Transportparameter dünner geträgerter Kathodenschichten der oxidkeramischen Brennstoffzelle**
von C. Wedershoven (2010), vi, 137 Seiten
ISBN: 978-3-89336-666-8

84. **Charakterisierung der Quellverteilung von Feinstaub und Stickoxiden in ländlichem und städtischem Gebiet**
von S. Urban (2010), vi, 211 Seiten
ISBN: 978-3-89336-669-9

85. **Optics of Nanostructured Thin-Film Silicon Solar Cells**
by C. Haase (2010), 150 pages
ISBN: 978-3-89336-671-2

86. **Entwicklung einer Isolationsschicht für einen Leichtbau-SOFC-Stack**
von R. Berhane (2010), X, 162 Seiten
ISBN: 978-3-89336-672-9

87. **Hydrogen recycling and transport in the helical divertor of TEXTOR**
by M. Clever (2010), x, 172 pages
ISBN: 978-3-89336-673-6

88. **Räumlich differenzierte Quantifizierung der N- und P-Einträge in Grundwasser und Oberflächengewässer in Nordrhein-Westfalen unter besonderer Berücksichtigung diffuser landwirtschaftlicher Quellen**
von F. Wendland et. al. (2010), xii, 216 Seiten
ISBN: 978-3-89336-674-3

89. **Oxidationskinetik innovativer Kohlenstoffmaterialien hinsichtlich schwerer Lufteinbruchstörfälle in HTR´s und Graphitentsorgung oder Aufarbeitung**
von B. Schlögl (2010), ix, 117 Seiten
ISBN: 978-3-89336-676-7

90. **Chemische Heißgasreinigung bei Biomassenvergasungsprozessen**
von M. Stemmler (2010), xv, 196 Seiten
ISBN: 978-3-89336-678-1

91. **Untersuchung und Optimierung der Serienverschaltung von Silizium-Dünnschicht-Solarmodulen**
von S. Haas (2010), ii, 202 Seiten
ISBN: 978-3-89336-680-4

92. **Non-invasive monitoring of water and solute fluxes in a cropped soil**
by S. Garré (2010), xxiv, 133 pages
ISBN: 978-3-89336-681-1

93. **Improved hydrogen sorption kinetics in wet ball milled Mg hydrides**
by L. Meng (2011), II, 119 pages
ISBN: 978-3-89336-687-3

94. **Materials for Advanced Power Engineering 2010**
ed. by J. Lecomte-Beckers, Q. Contrepois, T. Beck and B. Kuhn (2010), 1327 pages
ISBN: 978-3-89336-685-9

95. **2D cross-hole MMR – Survey design and sensitivity analysis for cross-hole applications of the magnetometric resistivity**
by D. Fielitz (2011), xvi, 123 pages
ISBN: 978-3-89336-689-7

96. **Untersuchungen zur Oberflächenspannung von Kohleschlacken unter Vergasungsbedingungen**
von T. Melchior (2011), xvii, 270 Seiten
ISBN: 978-3-89336-690-3

97. **Secondary Organic Aerosols: Chemical Aging, Hygroscopicity, and Cloud Droplet Activation**
by A. Buchholz (2011), xiv, 134 pages
ISBN: 978-3-89336-691-0

98. **Chrom-bezogene Degradation von Festoxid-Brennstoffzellen**
von A. Neumann (2011), xvi, 218 Seiten
ISBN: 978-3-89336-692-7

99. **Amorphous and microcrystalline silicon applied in very thin tandem solar cells**
by S. Schicho (2011), XII, 190 pages
ISBN: 978-3-89336-693-4

100. **Sol-gel and nano-suspension electrolyte layers for high performance solid oxide fuel cells**
by F. Han (2011), iv, 131 pages
ISBN: 978-3-89336-694-1

101. **Impact of different vertical transport representations on simulating processes in the tropical tropopause layer (TTL)**
by F. Plöger (2011), vi, 104 pages
ISBN: 978-3-89336-695-8

102. **Untersuchung optischer Nanostrukturen für die Photovoltaik mit Nahfeldmikroskopie**
von T. Beckers (2011), xiii, 128 Seiten
ISBN: 978-3-89336-696-5

103. **Impact of contamination on hydrogenated amorphous silicon thin films & solar cells**
by J. Wördenweber (2011), XIV, 138 pages
ISBN: 978-3-89336-697-2

104. **Water and Organic Nitrate Detection in an AMS: Laboratory Characterization and Application to Ambient Measurements**
by A. Mensah (2011), XI, 111 pages
ISBN: 978-3-89336-698-9

105. **Entwicklung eines neuen Konzepts zur Steuerung der thermischen Ausdehnung von glaskeramischen Verbundwerkstoffen mit angepasster Fließfähigkeit am Beispiel der Hochtemperatur-Brennstoffzelle**
von E. Wanko (2011), xi, 134 Seiten
ISBN: 978-3-89336-705-4

106. **Tomographic reconstruction of atmospheric volumes from infrared limb-imager measurements**
by J. Ungermann (2011), xiv, 153 pages
ISBN: 978-3-89336-708-5

107. **Synthese und Identifizierung von substituierten Mg-Al-Cl Doppelhydroxidverbindungen mit Schwerpunkt IR-Spektroskopie**
von B. Hansen (2011), XII, 121 Seiten
ISBN: 978-3-89336-709-2

108. **Analysis of spatial soil moisture dynamics using wireless sensor networks**
by U. Rosenbaum (2011), xxii, 120 pages
ISBN: 978-3-89336-710-8

109. **Optimierung von APS-ZrO2-Wärmedämmschichten durch Variation der Kriechfestigkeit und der Grenzflächenrauhigkeit**
von M. E. Schweda (2011), 168 Seiten
ISBN: 978-3-89336-711-5

110. **Sorption of a branched nonylphenol isomer and perfluorooctanoic acid on geosorbents and carbon nanotubes**
by C. Li (2011), X, 102 pages
ISBN: 978-3-89336-716-0

111. **Electron Transport in the Plasma Edge with Rotating Resonant Magnetic Perturbations at the TEXTOR Tokamak**
by H. Stoschus (2011), iv, 113 pages
ISBN: 978-3-89336-718-4

112. **Diffusion and Flow Investigations in Natural Porous Media by Nuclear Magnetic Resonance**
by N. Spindler (2011), viii, 144 pages
ISBN: 978-3-89336-719-1

113. **Entwicklung und Erprobung des Hygrometer for Atmospheric Investigations**
von T. Klostermann (2011), IV, 118 Seiten
ISBN: 978-3-89336-723-8

114. **Application of functional gene arrays for monitoring influences of plant/seasons on bacterial functions and community structures in constructed wetlands (Bitterfeld, Germany)**
by J. Ning (2011), xiv, 157 pages
ISBN: 978-3-89336-724-5

115. **Wasseraustrag aus den Kathodenkanälen von Direkt-Methanol-Brennstoffzellen**
von A. Schröder (2011), VII, 228 Seiten
ISBN: 978-3-89336-727-6

116. **CITYZEN Climate Impact Studies**
ed. by M. Schultz (2011), 45 pages
ISBN: 978-3-89336-729-0

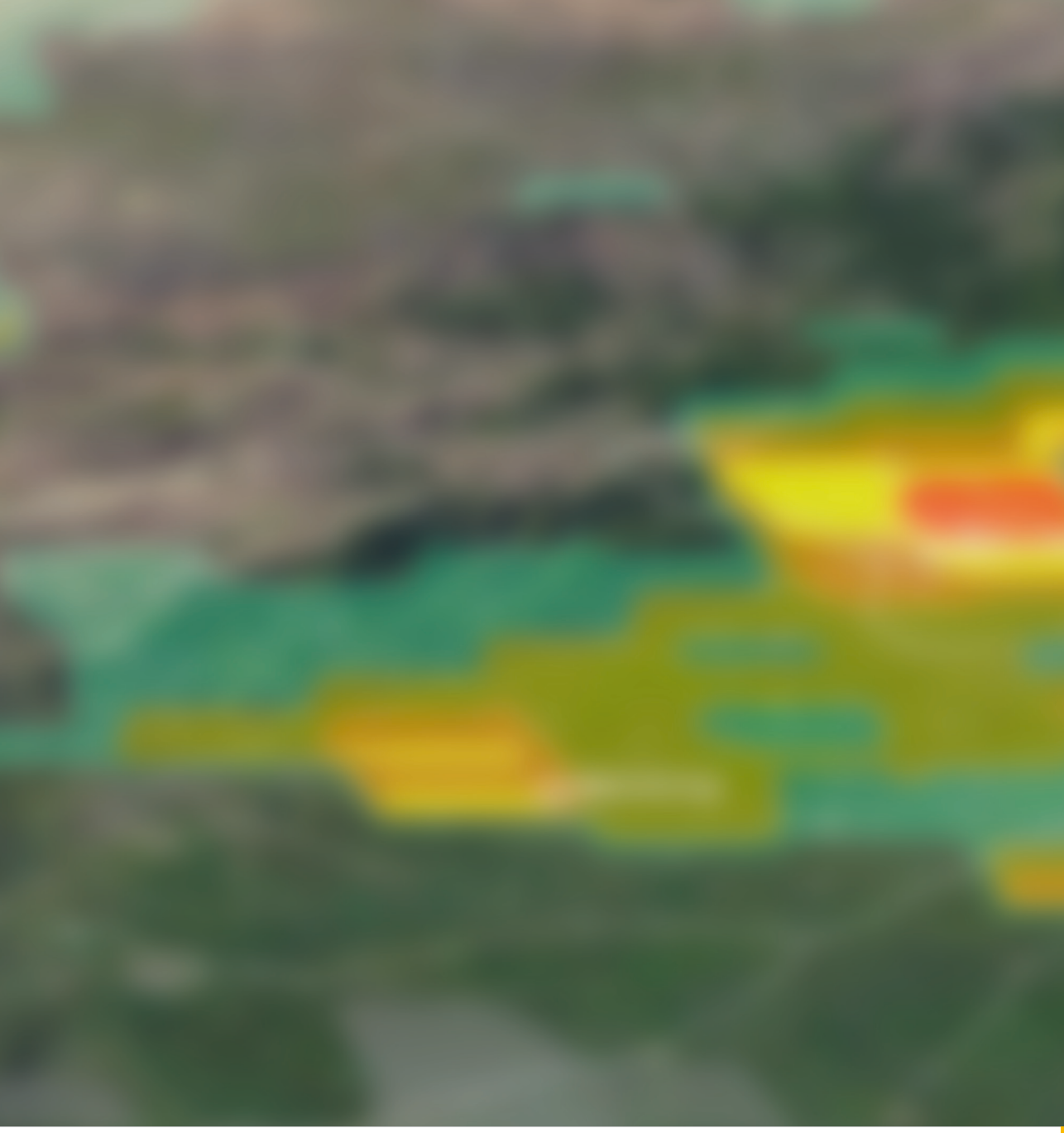

Energie & Umwelt / Energy & Environment
Band / Volume 116
ISBN 978-3-89336-729-0

JÜLICH
FORSCHUNGSZENTRUM